

**( $\alpha$ ,  $^8\text{Be}$ ) reaction in the  $1p$  shell\***

G. J. Wozniak, D. P. Stahel, and Joseph Cerny

*Department of Chemistry and Lawrence Berkeley Laboratory, University of California, Berkeley, California 94720*

N. A. Jelley

*Nuclear Physics Laboratory, University of Oxford, Oxford, England*

(Received 27 April 1976)

A  $^8\text{Be}$  identifier of high detection efficiency was utilized to investigate the ( $\alpha$ ,  $^8\text{Be}$ ) reaction on  $^{16}\text{O}$ ,  $^{15}\text{N}$ ,  $^{14}\text{N}$ ,  $^{13}\text{C}$ ,  $^{12}\text{C}$ ,  $^{11}\text{B}$ ,  $^{10}\text{B}$ , and  $^9\text{Be}$  targets at bombarding energies between 65 and 72.5 MeV. Differential cross sections were measured from  $\theta_{\text{c.m.}} = 20^\circ$ – $70^\circ$  for solid targets and over a more restricted range for the nitrogen gas targets. Excitation functions were obtained over a larger energy range for the  $^{12}\text{C}$  and  $^{16}\text{O}$  targets. At these energies, the ( $\alpha$ ,  $^8\text{Be}$ ) reaction was found to proceed predominantly via a direct  $\alpha$ -cluster pickup mechanism and to populate strongly only those levels consistent with this mechanism. The data were analyzed in the framework of the exact finite-range distorted-wave Born approximation. Absolute and relative  $\alpha$ -particle spectroscopic factors were extracted for 22 states. Good agreement was found between these experimental values and the theoretical predictions of Kurath and of Rotter for the extent of  $\alpha$  clustering in these light nuclei.

<p>NUCLEAR REACTIONS <math>^{16}\text{O}</math>, <math>^{15}\text{N}</math>, <math>^{14}\text{N}</math>, <math>^{13}\text{C}</math>, <math>^{12}\text{C}</math>, <math>^{11}\text{B}</math>, <math>^{10}\text{B}</math>, <math>^9\text{Be}(\alpha, ^8\text{Be})</math> <math>E_\alpha = 65</math>– 72.5 MeV; measured <math>\sigma(E_f, \theta)</math>; energy levels <math>^{12}\text{C}</math>, <math>^{11}\text{B}</math>, <math>^{10}\text{B}</math>, <math>^9\text{Be}</math>, <math>^8\text{Be}</math>, <math>^7\text{Li}</math>, <math>^6\text{Li}</math>, <math>^5\text{He}</math>; resolution 450 keV; DWBA analysis, deduced <math>S_\alpha</math> for 22 states, comparisons with theoretical <math>S_\alpha</math>.</p>
---

**I. INTRODUCTION**

The existence and the importance of multinucleon correlations in nuclei,<sup>1,2</sup> and in particular of  $\alpha$ -like four-nucleon correlations,<sup>3-7</sup> has intrigued physicists for decades. Recently, detailed theoretical calculations have been made of the extent of  $\alpha$  clustering in light nuclei<sup>8,9</sup> and several reactions have been employed to verify experimentally these predictions.<sup>10,11</sup>

Reactions involving the pickup or knockout of an  $\alpha$  particle are good probes of such correlations and in particular the ( $d$ ,  $^6\text{Li}$ ) (Refs. 12 and 13), ( $^3\text{He}$ ,  $^7\text{Be}$ ) (Refs. 14 and 15), and the ( $\alpha$ ,  $2\alpha$ ) (Ref. 16) reactions have been extensively utilized on light nuclei. Because of uncertainties in the parameters of the theoretical models used to describe these reactions, it is difficult to extract absolute  $\alpha$ -particle spectroscopic factors ( $S_\alpha$ ) from the measured cross sections. However, relative spectroscopic factors as well as information on the reaction mechanism have been obtained.

To complement the information acquired with the above three reactions, a very detailed study on  $1p$  shell targets has been made with the ( $\alpha$ ,  $^8\text{Be}$ ) reaction. This reaction has an *a priori* simplicity because the  $^8\text{Be}$  ground state looks very much like two  $\alpha$  particles weakly bound in a relative  $s$  state; further, since the projectile, the transferred  $\alpha$  particle, and the  $^8\text{Be}$  ground state all have zero spin, simple selection rules result. Although  $^8\text{Be}$

is particle-unstable ( $t_{1/2} \sim 10^{-16}\text{s}$ ), its ground state is long-lived compared with nuclear transit times, and one should be able to treat it as a single nucleus in a direct reaction. To investigate this sparsely utilized reaction,<sup>17,18</sup> a special identifier was developed<sup>19</sup> which detects the particle-unbound  $^8\text{Be}$  nucleus. Moreover, this identifier eliminated from the spectra any contributions from transitions to excited states of  $^8\text{Be}$ .

The present investigation was carried out at moderately high bombarding energies (65–72.5 MeV) where it was hoped that direct processes would dominate and thus make possible the extraction of experimental spectroscopic factors. All stable  $1p$  shell targets were investigated and the data were analyzed in the framework of the exact finite-range distorted-wave Born approximation (EFR-DWBA). In Sec. II the experimental method is described and in Sec. III the experimental results are presented. Absolute and relative  $S_\alpha$  were extracted and are compared with theoretical  $S_\alpha$  in Sec. IV. Finally, a summary and conclusions are presented in Sec. V.

**II. EXPERIMENTAL METHOD**

The study of reactions with  $^8\text{Be}$  nuclei as the detected particles is complicated by the fact that the  $^8\text{Be}$  ground state decays promptly, and must be observed indirectly by means of its breakup  $\alpha$  particles. The essential problem lies in detecting these

two particles with high efficiency, while at the same time accurately determining the energy and direction of the original  ${}^8\text{Be}$  event.

Detection systems for  ${}^8\text{Be}$  reaction products fall into two general categories: those which incorporate kinematic compensation<sup>19</sup> of the energy variation across the  ${}^8\text{Be}$  acceptance angle and those which do not.<sup>17,20-26</sup> The latter systems limit this energy spread by using collimators to define the  ${}^8\text{Be}$  acceptance angle while the former utilize a position-sensitive detector (PSD) to measure the  ${}^8\text{Be}$  direction and hence permit kinematic compensation. To obtain a large effective geometry, a  ${}^8\text{Be}$  detection system must subtend a large solid angle. Hence, methods which rely on collimation cannot simultaneously optimize both the efficiency and the energy resolution for light targets since a small acceptance angle is necessary for small kinematic broadening. However, if a PSD is used to measure both the direction and the energy of a  ${}^8\text{Be}$  event, the detection efficiency and the energy resolution may be optimized concurrently with no restriction on the acceptance angle.

A counter-telescope system capable of identifying  ${}^8\text{Be}$  events is outlined below; it incorporates a PSD as an  $E$  detector. To obtain selective  ${}^8\text{Be}$  identification, a subnanosecond coincidence between twin transmission ( $\Delta E$ ) detectors is employed. This technique permits low cross section reactions ( $\geq 0.1 \mu\text{b}/\text{sr}$ ) to be efficiently studied at high counting rates (50 000 cps). The  ${}^8\text{Be}$  identifier described in this paper incorporates a number of simplifying features and a larger effective solid angle (1 msr) than our previously reported design for such a system.<sup>19</sup>

#### A. ${}^8\text{Be}$ identifier

The decay of the  ${}^8\text{Be}$  ground state is characterized by a single decay channel, a small breakup energy ( $Q=0.092 \text{ MeV}$ ), two identical charged products ( $\alpha$  particles), and, since all the spins involved are zero, an isotropic distribution of the decay products in their center of mass. By designing a detection system for high-energy  ${}^8\text{Be}$  events [ $E({}^8\text{Be}) \equiv E_g > 35 \text{ MeV}$ ], advantage can be taken of the strong kinematic focusing of the  $\alpha$  particles into a narrow breakup cone (apex angle  $< 6^\circ$ ) whose axis lies in the direction of the original  ${}^8\text{Be}$  event. The distribution of the breakup  $\alpha$  particles is sharply peaked at the surface of the breakup cone; thus, in order to detect a substantial fraction of the  ${}^8\text{Be}$  events, a detector should subtend an angle larger than the opening angle of the cone. For a large angular acceptance ( $10^\circ$ ), a considerable variation in the detection angle ( $\theta_{\text{lab}}$ ) of the  ${}^8\text{Be}$  events is possible. On light targets ( $A \leq 16$ ), a

typical value of  $dE/d\theta$  near  $25^\circ$  (lab) for the ( $\alpha, {}^8\text{Be}$ ) reaction at  $E_\alpha \sim 65 \text{ MeV}$  is around 500 keV/deg. The substantial kinematic broadening that would occur can be compensated for by using a PSD.

A particle striking a position-sensitive detector generates both an energy signal  $E$ , and a signal  $XE$  proportional to the product of its energy  $E$  and its distance of impact  $X$  from one side of the detector; see Fig. 1. For high-energy  ${}^8\text{Be}$  events, the breakup  $Q$  value is small compared to the  ${}^8\text{Be}$  energy, and so the two breakup  $\alpha$  particles have, to a good approximation, equal energies. On striking a PSD, one  $\alpha$  particle produces a signal  $X_1E/2$ ; the other,  $X_2E/2$ . Since both  $\alpha$  particles arrive within a fraction of a nanosecond of one another, the individual  $E$  and  $XE$  signals are automatically summed and the resultant  $E$  signal gives the energy of the  ${}^8\text{Be}$  event. The position signal  $X$  obtained by dividing out the energy dependence is given by

$$X = (X_1E/2 + X_2E/2)/(E/2 + E/2) = (X_1 + X_2)/2.$$

In addition to having equal energies, the two  $\alpha$  particles are detected at approximately equal distances from the axis of the  ${}^8\text{Be}$  breakup cone, which corresponds to the direction of the original  ${}^8\text{Be}$  event as shown in Fig. 1. Since this average position  $X$  establishes the direction<sup>19</sup> of the  ${}^8\text{Be}$  event ( $\theta_{\text{lab}}$ ), substantial kinematic broadening can be compensated for by gating the energy signals with position signals corresponding to a small angular range.

While good efficiency and energy resolution can be obtained with a PSD alone, numerous particle-stable nuclei would also be detected and would obscure  ${}^8\text{Be}$  events except when the latter happened to be more energetic. To select only  ${}^8\text{Be}$  events,

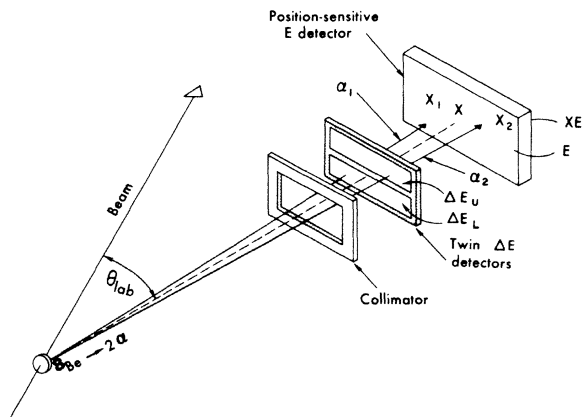


FIG. 1. A schematic diagram of the  ${}^8\text{Be}$  identifier showing the twin transmission detectors, the PSD, the trajectories of the breakup  $\alpha$  particles (solid lines) and the measured direction  $X$  of the  ${}^8\text{Be}$  event.

a twin transmission detector is placed in front of the PSD as shown in Fig. 1. This detector consists of a single silicon wafer with two  $\Delta E$  counters diffused side by side.<sup>27</sup> By making a subnanosecond coincidence between these detectors,  ${}^8\text{Be}$  events can be selectively observed as shown in Fig. 2(a). This fast coincidence not only eliminates particle-stable nuclei, but also eliminates inter-beam-burst chance coincidence events, which, because of the microscopic duty cycle of the cyclotron beam, come  $\sim 100$  ns apart.

In addition this subnanosecond coincidence also removes a substantial fraction of the intra-beam-burst pileup. When  ${}^8\text{Be}$  decays, the two breakup  $\alpha$  particles have approximately the same energy and thus their time-of-flight difference ( $\Delta\text{TOF}$ ) to the upper and lower  $\Delta E$  detectors is approximately zero. The full width at the base of the peak in Fig. 2(a) ( $2\Delta\text{TOF} = 0.85$  ns) illustrates the similar flight times of the two  $\alpha$  particles and the central dip is the effect of collimation on their velocity distribution.<sup>19</sup> By performing a subnanosecond coincidence between the upper and lower halves of the twin  $\Delta E$  detectors, the intra-beam-burst background can be reduced by a factor of 10, since the typical beam-burst width at the Berkeley 88-inch cyclotron is approximately 5 ns (at a frequency of 9 MHz). Some further reduction in background<sup>28</sup> and additional selection of  ${}^8\text{Be}$  events is obtained by performing particle identification with the summed  $\Delta E$  and  $E$  signals as shown in Fig. 2(b) ( ${}^8\text{Be}$  identifies as if it were a  ${}^7\text{Li}$  event<sup>18</sup>).

Since commercially available PSD's give position information along their longest dimension, the largest effective solid angle and kinematic compensation are obtained by orienting the twin transmission detector as shown in Fig. 1. In this configuration  ${}^8\text{Be}$  events can be detected over an angular spread of several degrees with an almost con-

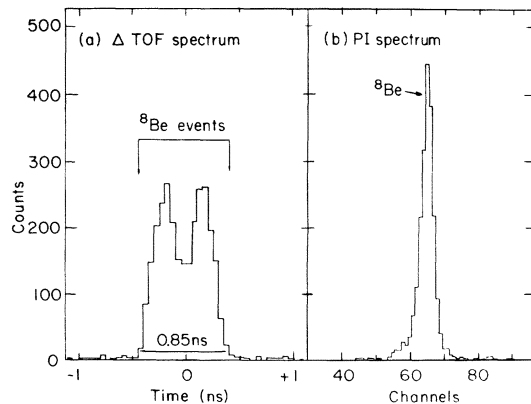


FIG. 2. Differential time of flight  $\Delta\text{TOF}$  (a) and particle identification PI (b) spectra obtained with the  ${}^8\text{Be}$  identifier.

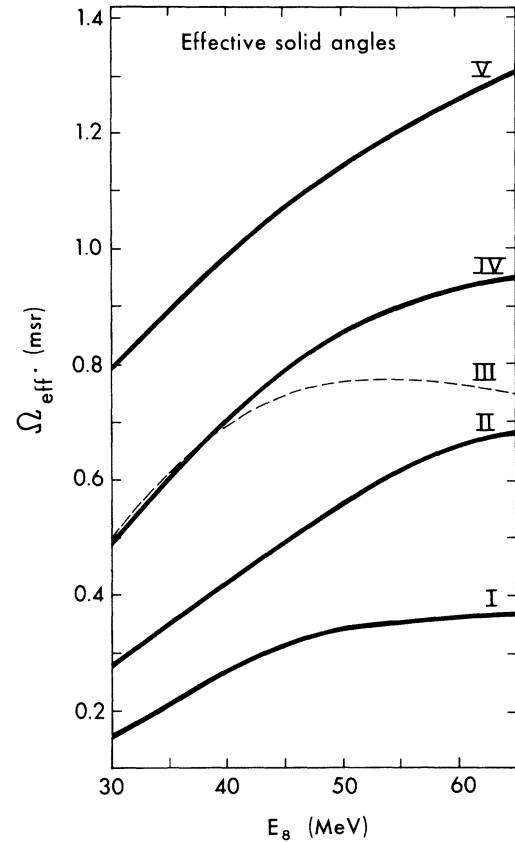


FIG. 3. The effective solid angles  $\Omega_{\text{eff}}$  of several different  ${}^8\text{Be}$  identifiers (I–V) which were used to study solid targets (solid lines) and gas targets (dashed line). See Table I for a description of the geometries of these identifiers.

stant detection efficiency. Characteristics of this particular geometry and the other geometries employed in the various experiments are given in Fig. 3 and Table I. Shown in Fig. 3 are the effective solid angles  $\Omega_{\text{eff}}$  for several identifier geometries as a function of the  ${}^8\text{Be}$  energy; Table I gives the geometry parameters employed. The effective solid angle decreases at lower energies because of the increasing size of the breakup cone ( $\Omega_{\text{eff}} = \epsilon\Omega_{\text{acc}}$  where  $\Omega_{\text{acc}}$  is the acceptance solid angle and  $\epsilon$  is the detection efficiency; see Ref. 19 for further details).

### B. Experimental procedure

The experiments discussed in this work utilized 55–72.5 MeV  $\alpha$ -particle beams from the Lawrence Berkeley Laboratory 88-inch cyclotron. Intensities of 1 to 2  $\mu\text{A}$  were readily delivered on target. Typical beam spot sizes were  $1.5 \times 2.0$  mm<sup>2</sup> and the beam energy resolution was 0.14%. To deflect low-energy electrons, an 800 G permanent magnet was

TABLE I.  $^8\text{Be}$  identifier geometry for several different experiments.

Experiment	Target to PSD distance (cm)	Collimator <sup>a</sup>	Diameter <sup>a</sup> (cm)	Width <sup>a</sup> (cm)	Height <sup>a</sup> (cm)	Post or <sup>b</sup> gap width (cm)	Position <sup>c</sup> gate width (cm)	Acceptance angle ( $^8\text{Be}$ ) (deg)
I	8.00	circular	0.83	...	...	0.28 (V)	0.12	0.9
II	13.00	rectangular	...	1.12	1.25	0.30 (V)	0.25	1.1
III	7.45	gas <sup>d</sup>	...	0.78	0.81	0.24 (V)	0.26	2.0
IV	13.35	rectangular	...	1.51	0.98	0.19 (V)	0.53	2.3
V	13.05	rectangular	...	2.00	0.99	0.09 (H)	1.07	4.7

<sup>a</sup> Projected dimensions of the collimator on the PSD.

<sup>b</sup> Projected dimension on the PSD of the divided collimator post width (Ref. 19) or the gap width of the undepleted region (Ref. 19) between the twin transmission detectors. The letters V or H indicate whether the gap was vertical (V) or horizontal (H).

<sup>c</sup> If more than one position gate was set, only the summed width is given.

<sup>d</sup> The distances from the target to the gas collimator ( $L_1$ ) and from this collimator to the second one ( $L_2$ ) were 3.60 and 3.85 cm, respectively. Only the dimensions of the second collimator are listed above. The dimensions of the width, height, and post of the front gas collimator were 0.38, 0.38, and 0.12 cm, respectively.

placed in front of the  $^8\text{Be}$  identifier, which was mounted on a platform inside a 0.51 m scattering chamber. A pressure of  $\sim 4 \times 10^{-5}$  Torr was maintained in this chamber and, to eliminate carbon buildup on the targets, a hollow cylindrical liquid nitrogen cold trap was placed along the beam axis immediately upstream from the target. The detectors were placed close to the target (8 to 13 cm) for good detection efficiency. Because several different versions of the  $^8\text{Be}$  identifier were employed in the course of these experiments, the effective solid angles varied from 0.15 to 1.3 msr (see Fig. 3 and Table I). An experimental  $^8\text{Be}$  energy resolution of 400 keV was obtained [important contributions to this arose from the radial width of the beam spot and from the high counting rate (50 000 cps)].

Self-supporting  $^9\text{Be}$ ,  $^{10}\text{B}$  (98%),  $^{11}\text{B}$  (98%),  $^{12}\text{C}$ ,  $^{13}\text{C}$  (90%), and  $\text{SiO}_2$  targets were used in these experiments. Table II gives the target thicknesses and the detection geometry employed in the particular measurement. Target thicknesses were determined by placing a thin  $^{212}\text{Pb}$  source behind each target and measuring the energy loss of the

$\alpha$  particles passing through it. In addition, for targets of natural isotopic composition, a 1 cm<sup>2</sup> central circular portion was punched out and weighed on a microbalance.

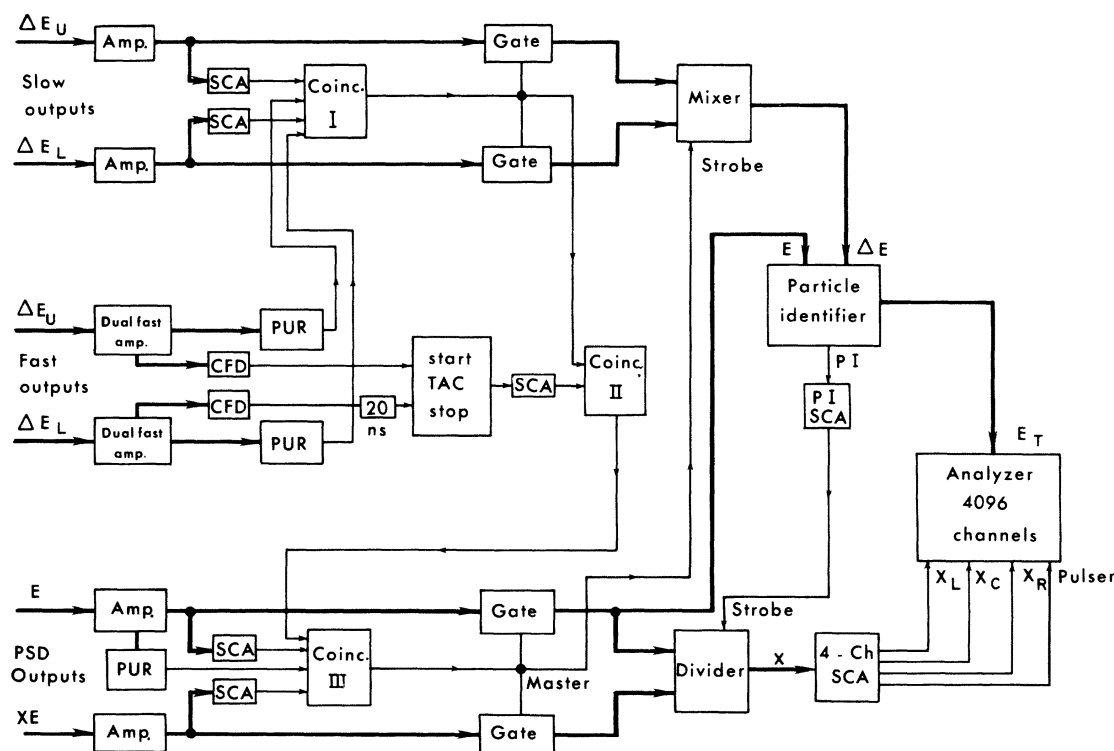
A gas target and recovery system was used in the experiments with chemically pure  $^{14}\text{N}_2$ ,  $^{16}\text{O}_2$ , and isotopically enriched  $^{15}\text{N}_2$  (99%) gases at a pressure of 0.3 atm. To define the extent of the gas target from which  $^8\text{Be}$  events could be observed, a second, more forward collimator was also used.<sup>19</sup> For this two-collimator system, the energy dependence of the detection efficiency was estimated using a simple correction to the calculation for a single collimator. Comparisons between data taken with oxygen gas targets and  $\text{SiO}_2$  targets were used to normalize the gas target cross sections.

Several surface-barrier position-sensitive detectors<sup>29</sup> with active areas of  $13 \times 20$ ,  $10 \times 30$ , and  $10 \times 50$  mm<sup>2</sup> and depletion depths ranging from 300 to 500  $\mu\text{m}$  were used. These PSD's all had position resolutions of 0.5% to 1% of their length. Their measured energy resolution was 70 keV full width

TABLE II. Solid and gas target thicknesses.

Experiment	$E_\alpha$ (MeV)	Solid targets ( $\mu\text{g}/\text{cm}^2$ )						Gas targets			
		$^9\text{Be}$	$^{10}\text{B}$	$^{11}\text{B}$	$^{12}\text{C}$	$^{13}\text{C}$	$^{16}\text{O}^a$	Pressure (atm)		Temperature ( $^\circ\text{C}$ )	
								$^{14}\text{N}_2$	$^{15}\text{N}_2$	$^{14}\text{N}_2$	$^{15}\text{N}_2$
I	65.0			100	50		220				
II	72.5		150	100	305		210				
III	72.5				305			0.33	0.27	27	27
IV	65.0	130			200	135	145				
V	60.0						240				

<sup>a</sup> Thickness of  $\text{SiO}_2$  targets.

FIG. 4. An electronic block diagram for the  ${}^8\text{Be}$  identifier.

at half maximum (FWHM) and the observed change in pulse height across their length was 100 keV for 8.78 MeV  $\alpha$  particles.

Fully depleted phosphorous-diffused transmission detectors with depletion depths of 100 to 200  $\mu\text{m}$  and active areas of 80 to 130  $\text{mm}^2$  were fabricated at the Lawrence Berkeley Laboratory. Typically, these detectors gave a good signal-to-noise ratio and held a large voltage gradient (2 V/ $\mu\text{m}$ ), ensuring fast ( $<1$  ns) collection of the deposited charge. Subnanosecond timing was possible with these detectors using preamplifiers mounted outside the chamber vacuum and simply connected to the detectors via a 50  $\Omega$  coaxial cable 40 cm in length. The preamplifiers gave both a fast and a charge-sensitive (slow) output and were similar to those described in Ref. 19 except that the first stage field-effect transistor was incorporated in the preamplifier.

As indicated in the block diagram of the electronics for the  ${}^8\text{Be}$  identifier shown in Fig. 4, the fast outputs of the  $\Delta E_L$  and  $\Delta E_U$  preamplifiers fed two constant-fraction discriminators (CFD), which were connected to a time-to-amplitude converter (TAC). The energy deposited in these  $\Delta E$  detectors by  $\alpha$  particles under our experimental conditions varied between 4 and 11 MeV, but no additional time-walk-with-amplitude compensation was required for good time resolution, since  ${}^8\text{Be}$  events

generate  $\Delta E_L$  and  $\Delta E_U$  signals of approximately equal amplitude. Pileup rejectors (PUR) on all three detectors eliminated inter-beam-burst chance-coincident events. A simulated 40 MeV  ${}^8\text{Be}$  event gave a time resolution of 200 ps FWHM. Particle identification PI, position X, and time-of-flight  $\Delta\text{TOF}$  gates were set with single channel analyzers (SCA's); energy spectra, gated by these parameters, and routed by position were collected on a 4096 channel analyzer. Gated PI, position, and  $\Delta\text{TOF}$  spectra were monitored during the experiments. Dead times were measured by comparing the number of pulser events (triggered by a monitor counter) in the spectrum to the number of pulser triggers.

During an experiment, energy spectra routed by up to four position gates were accumulated in 1024 channel groups of the multichannel analyzer. At the end of a run these data were transferred to an SCC-660 computer and written on magnetic tape. Upon completion of an experiment, analysis of these energy spectra was performed with an interactive, Gaussian peak-fitting program. The detection efficiency and effective solid angle for a  ${}^8\text{Be}$  event were calculated with the program EFFCR.<sup>30</sup>

### III. RESULTS

In analogy to the analysis of direct single-nucleon pickup reactions, one hopes that the main features

TABLE III. Experimental peak ( $\alpha$ ,  $^8\text{Be}$ ) cross sections for the population of a final state and the predicted  $\alpha$ -particle spectroscopic factor for transitions to that state.

Product nucleus	Known levels <sup>a</sup>			Observed levels		Peak cross section ( $\mu\text{b}/\text{sr}$ )	Kurath <sup>b</sup>	$S_\alpha$	Rotter <sup>c</sup>
	(MeV)	$J^\pi$	$T$	(MeV)	( $\pm\text{keV}$ )				
$^{12}\text{C}$	0	$0^+$	0	0		23	0.23	0.23	
	4.44	$2^+$	0	4.42	40	42	1.30	1.26	
	7.65	$0^+$	0	7.67	50	3.4	0.06		
	9.64	$3^-$	0	9.65	50	8.6			
	10.3	$(0^+)$	0			<1			
	10.84	$1^-$	0			<1			
	11.83	$2^-$	0			<1			
	12.71	$1^+$	0			<1			
	13.35	$(2^-)$	0			<1			
	14.08	$4^+$	0	14.06	100	13	2.38	2.44	
$^{11}\text{B}$	0	$\frac{3}{2}^-$	$\frac{1}{2}$	0		8.7	0.41		
	2.12	$\frac{1}{2}^-$	$\frac{1}{2}$	2.10	40	11	0.20		
	4.44	$\frac{5}{2}^-$	$\frac{1}{2}$	4.50	70	9.2	0.29		
	5.02	$\frac{3}{2}^-$	$\frac{1}{2}$				0.11		
	6.74	$\frac{7}{2}^-$	$\frac{1}{2}$	6.75	40	9.2	1.09		
	6.79	$\frac{1}{2}^+$	$\frac{1}{2}$						
	7.29	$(\frac{3}{2}, \frac{5}{2})^+$	$\frac{1}{2}$						
	7.98	$\frac{3}{2}^+$	$\frac{1}{2}$						
$^{10}\text{B}$	0	$3^+$	0	0		8.6	0.70		
	0.72	$1^+$	0			1.1	0.13		
	1.74	$0^+$	1						
	2.15	$1^+$	0	2.11	50	5.9	0.18		
	3.59	$2^+$	0	3.58	60	6.2	0.35		
	4.77	$3^+$	0	4.76	70	1.0	0.05		
	5.11	$2^-$	0						
	5.17	$2^+$	1						
	5.18	$1^+$	0				0.07		
	5.92	$2^+$	0						
	6.02	$4^+$		6.07	80	7.2	0.40		
	6.13	$3^-$							
$^9\text{Be}$	0	$\frac{3}{2}^-$	$\frac{1}{2}$	0		19.4	0.41		
	1.68	$\frac{1}{2}^+$	$\frac{1}{2}$						
	2.43	$\frac{5}{2}^-$	$\frac{1}{2}$	2.39	40	9.2	0.22		
	2.78	$\frac{1}{2}^-$	$\frac{1}{2}$			4	0.22		
	3.06	$\frac{5}{2}^+$	$\frac{1}{2}$						
	4.70	$(\frac{3}{2})^+$	$\frac{1}{2}$						
	6.76	$\frac{7}{2}^-$	$\frac{1}{2}$				0.23		
$^8\text{Be}$	0	$0^+$	0	0		50	0.56	0.54	
	2.94	$2^+$	0	2.96	70	75	0.71	0.68	
	11.4	$4^+$	0				0.77	0.68	
	16.63	$2^+$	$0+1$			<6	0.06		
	16.91	$2^+$	$0+1$						
$^7\text{Li}$	0	$\frac{3}{2}^-$	$\frac{1}{2}$	0		18.3	0.65	0.55	
	0.48	$\frac{1}{2}^-$	$\frac{1}{2}$	0.52	50	4.0	0.002		
	4.63	$\frac{7}{2}^-$	$\frac{1}{2}$	4.64	30	7.8	0.49	0.44	

TABLE III (Continued)

Product nucleus	Known levels <sup>a</sup>			Observed levels		Peak cross section ( $\mu\text{b}/\text{sr}$ )	Kurath <sup>b</sup>	$S_\alpha$	Rotter <sup>c</sup>
	(MeV)	$J^\pi$	$T$	(MeV)	( $\pm\text{keV}$ )				
${}^7\text{Li}$ (cont.)	6.68	$\frac{5}{2}^-$	$\frac{1}{2}$			3.0	0.08		
	7.47	$\frac{5}{2}^-$	$\frac{1}{2}$	7.46	70	2.6	0.07	0.06	
	9.61	$\frac{7}{2}^-$	$\frac{1}{2}$			<1			
	10.25	$\frac{3}{2}^-$	$\frac{1}{2}$			<1	0.005		
	11.25	$\frac{3}{2}^-$	$\frac{3}{2}$			<1			
${}^6\text{Li}$	0	$1^+$	0	0		6.2	0.003	0.013	
	2.18	$3^+$	0	2.18	30	28.6	1.06	0.37	
	3.56	$0^+$	1			<1			
	4.31	$2^+$	0			<1	0.06	0.36	
	5.37	$2^+$	1			<1			
	5.7	$1^+$	0			<1	0.01	0.37	
${}^5\text{He}$	0	$\frac{3}{2}^-$	$\frac{1}{2}$	0		87	1.12	1.15	
	4	$\frac{1}{2}^-$	$\frac{1}{2}$				0.06	0.03	
	16.76	$\frac{3}{2}^+$	$\frac{1}{2}$						

<sup>a</sup> See Refs. 31 and 32.<sup>c</sup> See Ref. 8.<sup>b</sup> See Ref. 9.

of the four-nucleon pickup reaction  $(\alpha, {}^8\text{Be})$  can be understood by assuming that the four nucleons are transferred as a single cluster having the internal quantum numbers of a free  $\alpha$  particle. For the nucleus  $B \rightarrow A + \alpha$ , the harmonic oscillator quantum numbers  $NL_\alpha$  describing the motion of the  $\alpha$  cluster with respect to the core  $A$  are given by the relation (assuming that the internal quantum numbers of the cluster are zero)

$$2(N-1) + L_\alpha = \sum_{i=1}^4 [2(n_i - 1) + l_i], \quad (1)$$

where  $n_i l_i$  are the shell model quantum numbers of the two protons and two neutrons which form the cluster. Thus, for  $\alpha$  clusters in the  $1p$  shell, the values of  $NL_\alpha$  are restricted to  $3S$ ,  $2D$ , and  $1G$ .

Since the projectile, the outgoing  ${}^8\text{Be}$  (treated as two  $\alpha$  particles in a relative  $s$  state) and the transferred cluster all have zero spin, quite restricted selection rules apply to the assumed simple direct reaction  $B(\alpha, {}^8\text{Be})A$ : for total angular momentum transfer  $\vec{J}$  and orbital angular momentum transfer  $\vec{L}$

$$\vec{J} = \vec{L} = \vec{J}_B - \vec{J}_A = \vec{L}_\alpha; \quad \Delta\pi = (-1)^L, \quad (2)$$

where  $\vec{L}_\alpha$  is the orbital angular momentum of an  $\alpha$  cluster in the target nucleus  $B$ . In addition the isospin change is given by  $\Delta T = 0$ . Thus for target nuclei having ground state spins of 0 or  $\frac{1}{2}$ , the transferred angular momentum  $L$  has a unique val-

ue for transitions to any final state. A summary of all the low excitation final states which possibly could be populated by the  $(\alpha, {}^8\text{Be})$  reaction in the  $1p$  shell is presented in Table III.<sup>31,32</sup> Measured excitation energies and peak cross sections are given and, where determined, upper limits are indicated for very weakly populated states. The theoretical spectroscopic factors<sup>8,9</sup> are also tabulated. If a final state can be populated by several different orbital angular momentum transfers, the sum  $S = \sum_{L_\alpha} S^{L_\alpha}$  is given. All final states populated by the  $(\alpha, {}^8\text{Be})$  reaction will be discussed below. The measured angular distributions will be presented with only statistical error bars on the data points; this indicates the relative error although the absolute cross sections could be in error by as much as 30%. Section IV discusses the fitting of the experimental angular distributions.

#### A. ${}^{16}\text{O}(\alpha, {}^8\text{Be}){}^{12}\text{C}$

Both  $\text{SiO}_2$  and oxygen gas targets were utilized in this investigation of the  ${}^{16}\text{O}(\alpha, {}^8\text{Be}){}^{12}\text{C}$  reaction. A  ${}^8\text{Be}$  energy spectrum ( $\theta_{\text{lab}} = 22.5^\circ$ ) obtained from a  $\text{SiO}_2$  target ( $145 \mu\text{g}/\text{cm}^2$ ) at a bombarding energy of 65 MeV is shown in Fig. 5. The observed energy resolution is 400 keV (FWHM) and transitions can be clearly seen to the ground and first excited states of  ${}^{12}\text{C}$ . Several small peaks due to  ${}^{28}\text{Si}$  or a  ${}^{12}\text{C}$  contaminant in the target appear between the two large peaks. The  $4^+$  14.08 MeV level<sup>31</sup> in  ${}^{12}\text{C}$

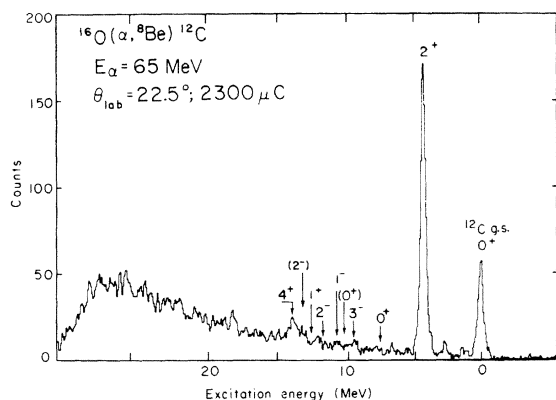


FIG. 5. An energy spectrum from the  $^{16}\text{O}(\alpha, ^8\text{Be})^{12}\text{C}$  reaction at  $\theta_{\text{lab}} = 22.5^\circ$ . The locations of possible transitions to all final states in  $^{12}\text{C}$  below 14 MeV excitation are indicated.

is only weakly populated at this angle; however, transitions to it were observed consistently with moderate strength (see Fig. 6) at most angles. Both the  $0^+$  7.65 MeV level and the  $3^-$  9.64 MeV level are not significantly populated at  $22.5^\circ$  al-

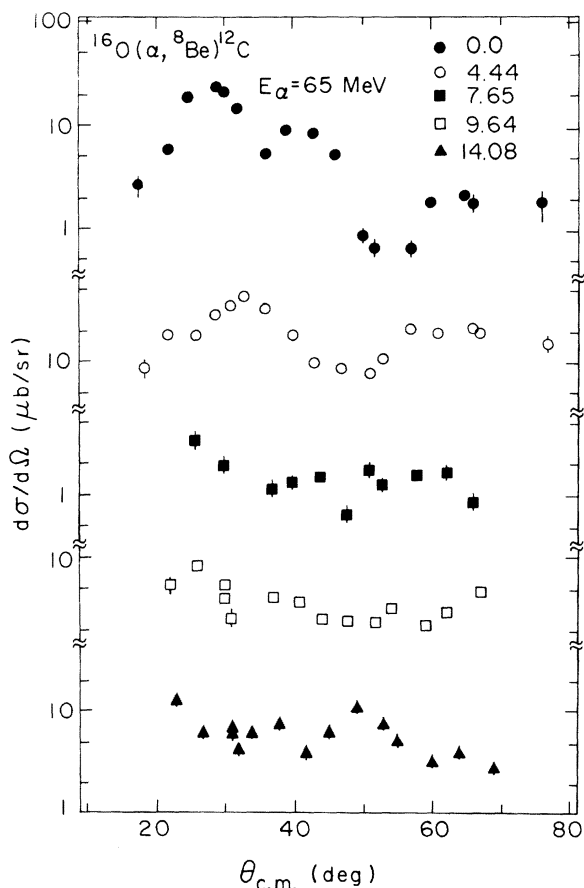


FIG. 6. Angular distributions for  $(\alpha, ^8\text{Be})$  transitions to the ground and four excited states of  $^{12}\text{C}$  at  $E_\alpha = 65$  MeV.

though they were regularly observed with weak strength (see Fig. 6). Furthermore, over the angular region investigated, no evidence was discerned for the population of the  $2^-$  11.83 MeV or  $1^+$  12.71 MeV unnatural parity states, the  $1^-$  10.84 MeV level, or the  $T=1$  states above 15 MeV excitation.

The observed weak population of the  $3^-$  9.64 MeV states requires an  $L=3$  transfer for the simplest case of  $\alpha$ -particle pickup. According to Eqs. (1) and (2) such a transfer is impossible if all four particles are transferred within the  $1p$  shell. However, this state may be formed via known  $2p$ - $2h$  and  $4p$ - $4h$  admixtures<sup>33</sup> in the ground state wave function of  $^{16}\text{O}$  or via possible<sup>34</sup>  $1s$  shell components in the  $^{12}\text{C}$   $3^-$  state wave function. Alternatively, the  $3^-$  state could be excited in a multistep or compound nucleus process so that its relative population may give an indication of the importance of such a process relative to a direct transfer. It should be noted that the ratio of the peak cross section of the  $3^-$  relative to the ground state at this energy is 0.37, whereas at lower bombarding energies<sup>17</sup> this ratio was observed to be  $\sim 1$ .

Angular distributions of the  $(\alpha, ^8\text{Be})$  reactions to the  $^{12}\text{C}(\text{g.s.})$ , 4.44, 7.65, 9.64, and 14.08 MeV states are given in Fig. 6. Both the  $L=0$  ground state transition and the  $L=2$  transition to the 4.44 MeV level show oscillatory behavior. The angular distributions for the three higher excited states are fairly structureless with the cross sections increasing slightly at forward angles.

#### B. $^{15}\text{N}(\alpha, ^8\text{Be})^{11}\text{B}$

At an incident energy of 72.5 MeV, the  $^{15}\text{N}(\alpha, ^8\text{Be})^{11}\text{B}$  reaction was studied with a simple identifier<sup>19</sup> which did not require a subnanosecond coincidence between the two  $\Delta E$  detectors. In Fig. 7(a) is shown a typical spectrum obtained at a gas pressure of 0.27 atm. Because the effective area of the PSD used in this experiment was only  $10 \times 10 \text{ mm}^2$ , it was necessary to place the counter telescope close to the gas cell wall to obtain a reasonable detection efficiency (see Table I). The resulting extended target, along with straggling in the cell windows, caused the poor energy resolution of  $\sim 800$  keV. The  $\frac{3}{2}^-$  ground,  $\frac{1}{2}^-$  2.12 MeV,  $\frac{5}{2}^-$  4.44 MeV, and  $\frac{7}{2}^-$  6.74 MeV states<sup>31</sup> have large theoretical  $S_\alpha$  (see Table III) and strong transitions are seen at these excitation energies in Fig. 7(a). Although the  $\frac{5}{2}^-$  4.44 MeV and  $\frac{3}{2}^-$  5.02 MeV levels are not resolved in this spectrum, they were resolved at  $\theta_{\text{lab}} = 15^\circ$  showing population of the former. In addition, the measured excitation energy of  $4.50 \pm 0.07$  MeV for this combined peak indicates that the  $\frac{5}{2}^-$  state (which has the larger theoretical  $S_\alpha$ ) was systematically populated more strongly than the  $\frac{3}{2}^-$  state.



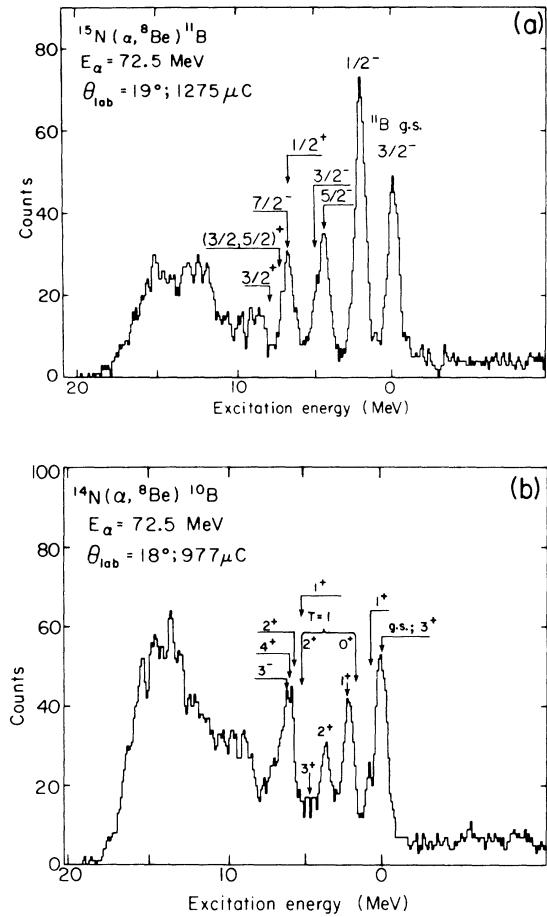


FIG. 7.  ${}^8\text{Be}$  energy spectra from (a) the  ${}^{15}\text{N}(\alpha, {}^8\text{Be}){}^{11}\text{B}$  and (b) the  ${}^{14}\text{N}(\alpha, {}^8\text{Be}){}^{10}\text{B}$  reactions at a bombarding energy of 72.5 MeV and laboratory angles of  $19^\circ$  and  $18^\circ$ , respectively. The locations of possible transitions to all final states below  $\sim 7$  MeV are shown.

No evidence was observed for transitions to the two positive parity states at 7.29 and 7.98 MeV. Thus a third positive parity level at 6.79 MeV was *assumed* not to be populated, and transitions to the peak observed at 6.75 MeV are attributed to the expected strong transition to the known  $\frac{7}{2}^-$  level at 6.74 MeV.

Angular distributions corresponding to transitions to the first four peaks of Fig. 7(a) are discussed in Sec. IV. Since the  ${}^{15}\text{N}$  ground state has a  $J^\pi$  of  $\frac{1}{2}^-$ , transitions to all final states in  ${}^{11}\text{B}$  should correspond to unique  $L$  values; however, no strong oscillatory behavior was observed.

### C. ${}^{14}\text{N}(\alpha, {}^8\text{Be}){}^{10}\text{B}$

A brief survey of the  $(\alpha, {}^8\text{Be})$  reaction on a  ${}^{14}\text{N}_2$  gas target was carried out at an incident energy of 72.5 MeV with the same identifier<sup>19</sup> as for  ${}^{15}\text{N}$ . Three angles were studied between  $\theta_{\text{lab}} = 18^\circ - 28^\circ$

with an energy resolution of  $\sim 800$  keV. An energy spectrum taken at  $\theta_{\text{lab}} = 18^\circ$  is shown in Fig. 7(b); the predicted locations of transitions to states below  $\sim 6$  MeV excitation are indicated. No evidence was observed for the excitation of the  $T=1$  states<sup>32</sup> occurring at 1.74 and 5.17 MeV in accordance with the  $\Delta T=0$  selection rule. Strong transitions were observed to the  $3^+$  ground;  $1^+$  2.15 MeV; and  $2^+$  3.59 MeV states, all of which have reasonably large theoretical  $S_\alpha$  (see Table III). The observed state at  $6.07 \pm 0.08$  MeV may correspond to the known  $4^+$  level at 6.02 MeV which has a large theoretical  $S_\alpha$ . A weak transition was observed to the  $1^+$  0.72 MeV state and a very weak one to the  $3^+$  4.77 MeV state; no transitions above background were observed to the  $1^+$  5.18 MeV state, which has a small theoretical  $S_\alpha$ .

The available angular distribution data span a very limited angular range and are discussed in Sec. IV. Over this restricted region the magnitudes

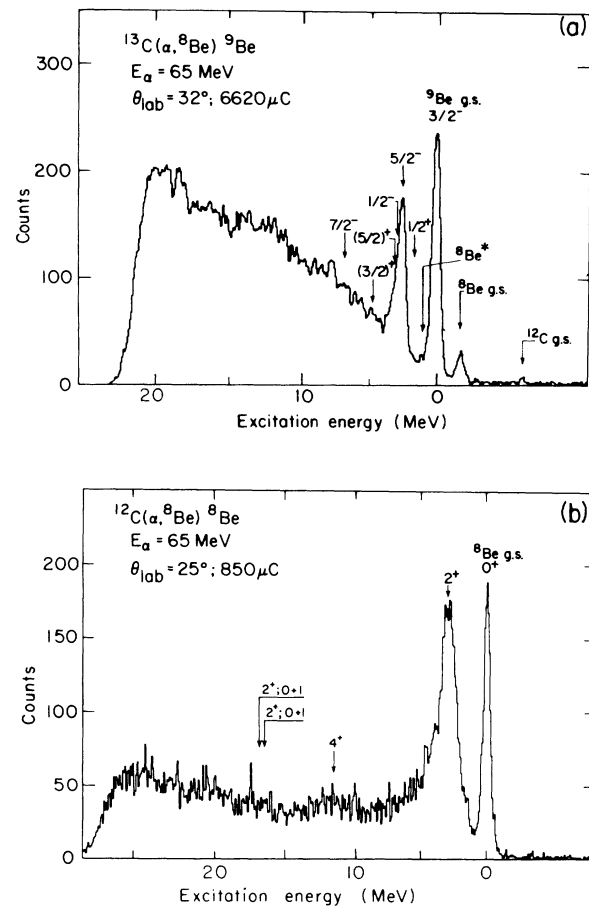


FIG. 8.  ${}^8\text{Be}$  energy spectra from (a) the  ${}^{13}\text{C}(\alpha, {}^8\text{Be}){}^9\text{Be}$  reaction at  $\theta_{\text{lab}} = 32^\circ$  and (b) the  ${}^{12}\text{C}(\alpha, {}^8\text{Be}){}^8\text{Be}$  reaction at  $\theta_{\text{lab}} = 25^\circ$  at a bombarding energy of 65 MeV. The locations of possible transitions to all final states in  ${}^9\text{Be}$  below  $\sim 7$  MeV and in  ${}^8\text{Be}$  below  $\sim 17$  MeV are indicated.

of the experimental angular distributions for the four strongly populated states are similar.

#### D. $^{13}\text{C}(\alpha, ^8\text{Be})^9\text{Be}$

A representative spectrum of the  $^{13}\text{C}(\alpha, ^8\text{Be})^9\text{Be}$  reaction induced by 65 MeV  $\alpha$  particles and with an energy resolution of 480 keV is shown in Fig. 8(a). A  $135 \mu\text{g}/\text{cm}^2$  self-supporting  $^{13}\text{C}$  target was used. There are four states in  $^9\text{Be}$  below 7 MeV excitation which have large theoretical  $S_\alpha$ . Strong transitions to two of these levels (the  $\frac{3}{2}^-$  ground state and the  $\frac{5}{2}^-$  second excited state<sup>32</sup>) dominate the experimental spectrum. As expected for the pickup of an  $\alpha$  cluster in the  $1p$  shell, the  $\frac{1}{2}^+$  1.68 MeV state is not populated nor is the  $(\frac{3}{2})^+$  level at 4.70 MeV. If the additional positive parity  $\frac{5}{2}^+$  3.06 MeV level was also not populated, transitions to the broad  $\frac{1}{2}^-$  2.78 MeV state account for the small shoulder on the  $\frac{5}{2}^-$  2.43 MeV peak. Transitions to the broad ( $\Gamma=2.0$  MeV)  $\frac{7}{2}^-$  6.76 MeV peak could not be observed above background. Since the  $^{13}\text{C}$  ground state has a  $J^\pi = \frac{1}{2}^-$ , transitions to all final states in  $^9\text{Be}$  correspond to unique  $L$  values. Angular distributions for the  $L=2$  transitions to the  $\frac{3}{2}^-$  and  $\frac{5}{2}^-$  levels are given in Sec. IV; quite flat distributions were observed.

#### E. $^{12}\text{C}(\alpha, ^8\text{Be})^8\text{Be}$

A  $^8\text{Be}$  energy spectrum of the  $^{12}\text{C}(\alpha, ^8\text{Be})^8\text{Be}$  reaction taken at  $\theta_{\text{lab}}=25^\circ$  is shown in Fig. 8(b). This spectrum was obtained by bombarding a  $200 \mu\text{g}/\text{cm}^2$  carbon target with 65 MeV  $\alpha$  particles. The observed energy resolution of the  $^8\text{Be}$  ground state peak in Fig. 8(b) is 450 keV. Transitions can clearly be seen to the  $0^+$  ground and  $2^+$  first excited states<sup>32</sup> with possible evidence for weak population of the broad ( $\Gamma \sim 3.5$  MeV)  $4^+$  level at 11.4 MeV. At  $E_\alpha = 72.5$  MeV stronger evidence was observed for the population of this  $4^+$  level. However, the  $2^+$  (mixed isospin) states at 16.63 and 16.91 MeV were not observably populated; Marion and Wilson<sup>35</sup> have shown that these states have a dominant single particle nature. An upper limit of 10% of the ground state strength could be placed on the population of these mixed isospin levels which is consistent with their small theoretical  $S_\alpha$  relative to that of the ground state (see Table III).

Experimental angular distributions of the transitions to the ground and first excited states of  $^8\text{Be}$  are discussed in Sec. IV. The  $L=0$  and  $L=2$  transfer both show oscillatory behavior.

#### F. $^{11}\text{B}(\alpha, ^8\text{Be})^7\text{Li}$

The  $^{11}\text{B}(\alpha, ^8\text{Be})^7\text{Li}$  reaction was investigated briefly at  $E_\alpha = 72.5$  MeV ( $\theta_{\text{lab}}=20^\circ$ ) and more com-

pletely at  $E_\alpha = 65$  MeV. Target thicknesses are given in Table II. Results at both energies are very similar and the  $^8\text{Be}$  energy spectrum obtained at the higher energy is shown in Fig. 9(a). Strong transitions to the  $\frac{3}{2}^-$  ground and  $\frac{7}{2}^-$  4.63 MeV states<sup>32</sup> are observed and weak ones to the  $\frac{1}{2}^-$  0.48 MeV state and the two  $\frac{5}{2}^-$  states at 6.68 and 7.47 MeV. The ground and first excited states are poorly resolved and there is a sizable uncertainty (20%) in the strength of the transition to the latter although it is populated with surprising strength (see Table III). States above 8 MeV excitation are very weakly populated and an upper limit of  $\sim 6\%$  of the ground state strength can be determined for these states. This limit is consistent with the small calculated  $S_\alpha$  for the  $\frac{3}{2}^-$  10.25 MeV state and the  $\Delta T=0$  selection rule which forbids populating the  $\frac{3}{2}^-$   $T = \frac{3}{2}$  11.25 MeV state.

At 65 MeV, angular distributions were obtained for the strong transitions populating the  $\frac{3}{2}^-$  ground and  $\frac{7}{2}^-$  4.63 MeV states of  $^7\text{Li}$ . These transitions involve two  $L$  transfers and the angular distributions (see Sec. IV) are rather structureless with an almost constant amplitude.

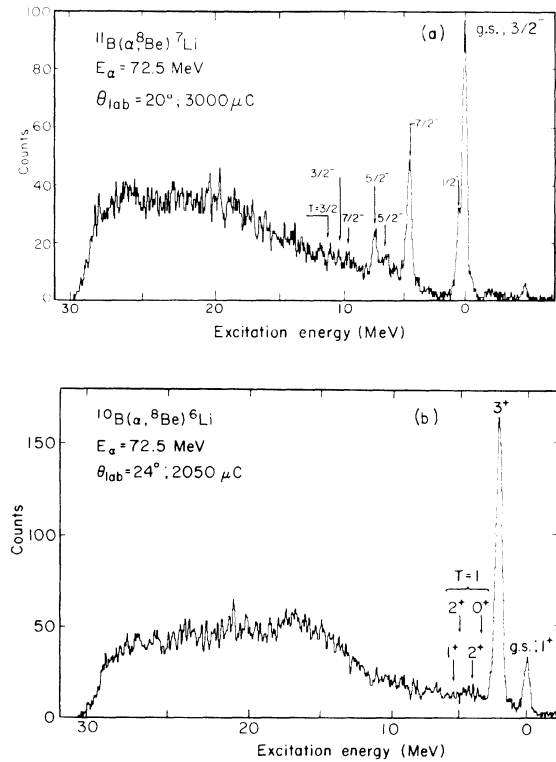


FIG. 9.  $^8\text{Be}$  energy spectra from (a) the  $^{11}\text{B}(\alpha, ^8\text{Be})^7\text{Li}$  reaction at  $\theta_{\text{lab}}=20^\circ$  and (b) the  $^{10}\text{B}(\alpha, ^8\text{Be})^6\text{Li}$  reaction at  $\theta_{\text{lab}}=24^\circ$ , both employed a bombarding energy of 72.5 MeV. The locations of possible transitions to all final states in  $^7\text{Li}$  below  $\sim 12$  MeV and in  $^6\text{Li}$  below  $\sim 6$  MeV are indicated.

G.  ${}^{10}\text{B}(\alpha, {}^8\text{Be}){}^6\text{Li}$ 

An investigation of this reaction was carried out by bombarding a  $150 \mu\text{g}/\text{cm}^2$  self-supporting  ${}^{10}\text{B}$  (98%) target with 72.5 MeV  $\alpha$  particles. As seen in Fig. 9(b) only two  ${}^6\text{Li}$  levels,<sup>32</sup> the  $1^+$  ground state and the  $3^+$  2.18 MeV level are observed. This spectrum is dominated by transitions to the  $3^+$  level which has a large theoretical  $S_\alpha$  (see Table III). Predicted locations for transitions to the  $2^+$  4.31 MeV and  $1^+$  5.7 MeV states and the  $T=1$  states at 3.56 and 5.37 MeV are also indicated. An upper limit of 4% of the strength to the first excited state can be set on the population of these levels. Kurath<sup>9</sup> predicts small  $S_\alpha$  for the former two states, while Rotter's<sup>8</sup> predicted large  $S_\alpha$  are inconsistent with the experimental evidence (see Table III). Transitions to the  $T=1$  states are forbidden by the  $\Delta T=0$  selection rule. It should be noted that the  ${}^6\text{Li}(\text{g.s.})$  is populated fairly weakly in accordance with its small  $S_\alpha$  (see Table III). The angular distributions of the transitions to both the ground and first excited states of  ${}^6\text{Li}$  have an almost constant amplitude (see Sec. IV). Due to the  $3^+$  spin of the  ${}^{10}\text{B}(\text{g.s.})$ , multiple  $L$  values are allowed in both of these transitions.

H.  ${}^9\text{Be}(\alpha, {}^8\text{Be}){}^5\text{He}$ 

The  ${}^9\text{Be}(\alpha, {}^8\text{Be}){}^5\text{He}$  reaction was observed at several forward angles at a bombarding energy of 65 MeV. In Fig. 10 is shown a  ${}^8\text{Be}$  energy spectrum which was obtained at  $\theta_{\text{lab}}=24^\circ$  by irradiating an  $130 \mu\text{g}/\text{cm}^2$   ${}^9\text{Be}$  target. Only the  $\frac{3}{2}^-$  ground state<sup>32</sup> of  ${}^5\text{He}$ , which has a large theoretical  $S_\alpha$ , was observed (see Table III). The  $\frac{1}{2}^-$  4 MeV level, which has a small  $S_\alpha$ , is difficult to observe because of the large background and its broad width ( $\Gamma=4$  MeV). The narrow  $\frac{3}{2}^+$  16.76 MeV level is not a

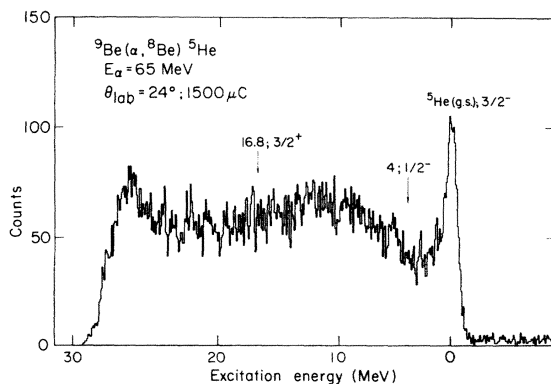


FIG. 10. An energy spectrum from the  ${}^9\text{Be}(\alpha, {}^8\text{Be}){}^5\text{He}$  reaction at  $\theta_{\text{lab}}=24^\circ$  and  $E_\alpha=65$  MeV. The locations of possible transitions to all final states in  ${}^5\text{He}$  below  $\sim 17$  MeV excitation are indicated.

simple  $1p$  shell state and, as expected, is not observably populated.

## I. Excitation functions

A direct reaction mechanism should give rise to a smooth variation of the shape and magnitude of the differential cross section with increasing bombarding energy. To determine in particular the nature of the  ${}^{12}\text{C}(\alpha, {}^8\text{Be}){}^8\text{Be}$  ground state reaction near 65 MeV, an excitation function was studied and measurements in small angular steps were taken over the maximum in the angular distribution near  $\theta_{\text{c.m.}}=35^\circ$ . Data obtained at  $E_\alpha=63.2, 65.2, 65.8, 66.6,$  and  $67.3$  MeV are shown in Fig. 11(a). The angular width of each data point is  $\sim 1^\circ$  and the error bars shown are statistical. Upon examining Fig. 11(a), it is clear that the magnitude of the differential cross section is a smooth and slowly decreasing function of the bombarding energy. The shape of the two observed maxima varies slowly with the incident energy.

An excitation function of the  $(\alpha, {}^8\text{Be})$  reaction on  ${}^{16}\text{O}$  was also established [see Fig. 11(b)]. Transitions to the ground state of  ${}^{12}\text{C}$  were measured at incident  $\alpha$  energies of 55, 60, 65, and 72.5 MeV. The behavior of the data taken at  $E_\alpha=65$  and 72.5 MeV, the latter over a limited angular region, is similar to that observed on  ${}^{12}\text{C}$ . However, the angular distribution at 55 MeV is quite different from that at the higher two energies and 60 MeV may be a transition region. Thus, at  $E_\alpha=55$  MeV, processes other than direct ones could be important in the  ${}^{16}\text{O}(\alpha, {}^8\text{Be}){}^{12}\text{C}$  ground state reaction; this was the conclusion reached by Brown *et al.*<sup>17</sup> for incident energies over the range 35–42 MeV. It is possible, of course, that this difference partly reflects a strong dependence of the direct transfer amplitude on the entrance channel optical potential and on the momentum distribution<sup>36</sup> of the bound  $\alpha$  particle in  ${}^{16}\text{O}$ . However, it would appear from the overall spectroscopic selectivity that we observe and the behavior of the angular distributions at 65 MeV and above that the reaction is predominantly direct in this energy region.

J. Comparison of  $(\alpha, {}^8\text{Be})$ ,  $(d, {}^6\text{Li})$ ,  $({}^3\text{He}, {}^7\text{Be})$ , and  $(\alpha, 2\alpha)$  reactions

The relative population of final states by the  $(\alpha, {}^8\text{Be})$  reaction on  $1p$  shell nuclei is in general in good agreement with the previously reported  $(d, {}^6\text{Li})$  and  $({}^3\text{He}, {}^7\text{Be})$  results at high bombarding energies<sup>15,37</sup> and with the assumption that these reactions proceed via a direct  $\alpha$ -cluster transfer. Only final states with the same parity as the target were appreciably populated with the notable exception of the  $3^-$  9.64 MeV level in  ${}^{12}\text{C}$ , which was

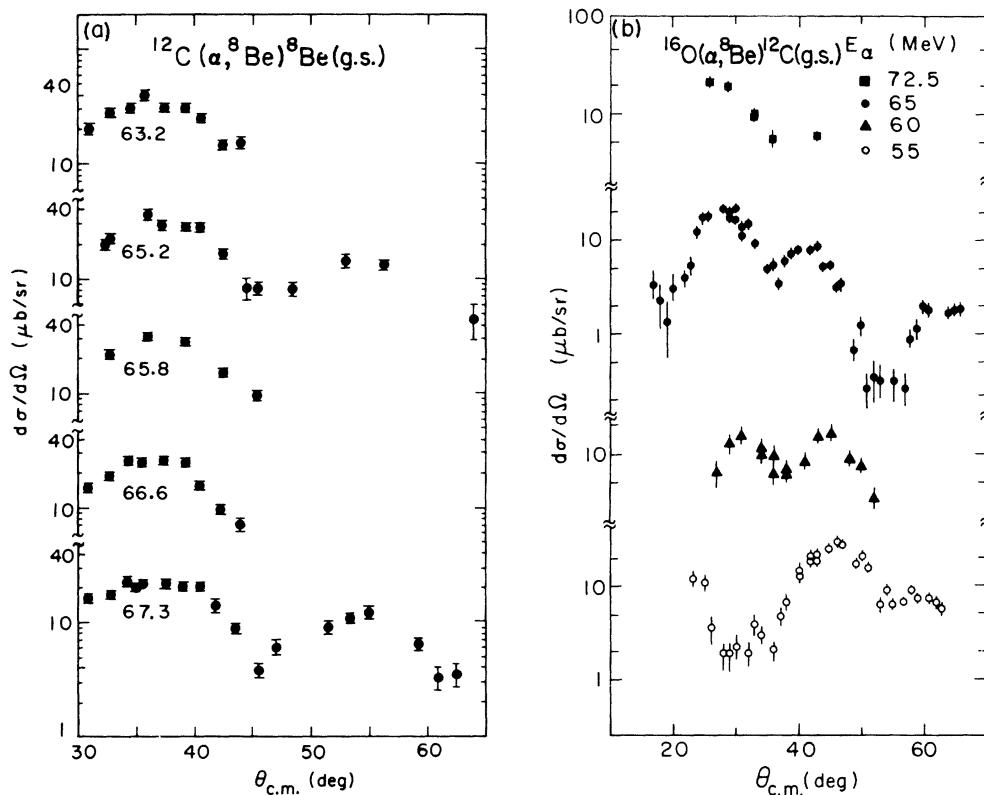


FIG. 11. Angular distributions of (a) the  $^{12}\text{C}(\alpha, ^8\text{Be})^8\text{Be}(\text{g.s.})$  reaction between  $E_\alpha = 63.2$  and  $67.3$  MeV and of (b) the  $^{16}\text{O}(\alpha, ^8\text{Be})^{12}\text{C}(\text{g.s.})$  reaction between  $E_\alpha = 55$  and  $72.5$  MeV. The angular width of each data point is  $\sim 1^\circ$  and a statistical error bar is shown if it exceeds the size of the data point.

made with moderate strength by all three reactions. In general the three pickup reactions strongly populated only final states with significant theoretical  $S_\alpha$ . Transitions to the mixed isospin  $2^+$  levels at 16.63 and 16.91 MeV in  $^8\text{Be}$  comprise an exception to this rule. These levels were not seen in the  $(\alpha, ^8\text{Be})$  reaction, as expected from their very small  $\alpha$ -particle spectroscopic factors, whereas both the  $(d, ^6\text{Li})$  and  $(^3\text{He}, ^7\text{Be})$  reactions populated them with moderate strength. From a comparison of the  $1p$  shell systematics for these  $\alpha$ -pickup reactions, it seems clear that a direct mechanism dominates at high energies. However, the  $(\alpha, ^8\text{Be})$  reaction appears to be somewhat more selective in populating predominantly final states with the same parity as the target and in only populating levels with large  $\alpha$ -particle spectroscopic factors.

Since the  $(\alpha, ^8\text{Be})$  and the  $(\alpha, 2\alpha)$  reactions share the same entrance channel and have very similar exit channels, it is interesting to compare these reactions on  $^{12}\text{C}$  and  $^{16}\text{O}$  targets. A very prominent systematic feature observed in a study of the  $(\alpha, 2\alpha)$  reaction on even-even  $1p$  shell and  $2s1d$  shell targets at  $E_\alpha = 90$  MeV (Ref. 16) was the pre-

dominance of the ground state transition at the symmetric quasielastic angle. In fact the  $^8\text{Be}$  and  $^{12}\text{C}$  ground states were observed in the  $(\alpha, 2\alpha)$  data to be populated a factor of 2 and 4, respectively, larger than their first excited states. In contrast, the  $(d, ^6\text{Li})$ ,  $(^3\text{He}, ^7\text{Be})$ , and  $(\alpha, ^8\text{Be})$  reactions all preferentially populated the  $^8\text{Be}(2.94$  MeV) state larger than its ground state and populated the  $^{12}\text{C}(4.44$  MeV) state a factor of 3 to 4 times stronger than its ground state. This apparent disagreement has been resolved by Chant and Roos<sup>38</sup> who showed that the low excited state cross sections were the result of distortion effects.

#### IV. ANALYSIS AND DISCUSSION

The selectivity of final states populated by the  $(\alpha, ^8\text{Be})$  reaction and the smooth dependence of the shape of its differential cross section on the bombarding energy (at or above 65 MeV) imply that this reaction can be analyzed in the framework of direct reaction theory, i.e., via the distorted-wave Born approximation (DWBA). The application of this theory is based on the assumption that the reaction proceeds by a one step pickup of an  $\alpha$

cluster" (two correlated protons and neutrons in an  $S = T = 0$  state).

#### A. DWBA calculations

In the distorted-wave Born approximation, the differential cross section for the reaction  $B(\alpha, {}^8\text{Be})A$  is given by

$$\frac{d\sigma}{d\Omega}(\theta) = \sum_L S^L(B - A + \alpha)S({}^8\text{Be} \rightarrow \alpha + \alpha)\sigma_{\text{DWBA}}^L(\theta), \quad (3)$$

where  $L$  runs over all the allowed angular momentum transfers according to Eq. (2). The kinematic part of the cross section,  $\sigma_{\text{DWBA}}^L$ , was calculated using DeVries's EFR-DWBA code LOLA.<sup>39</sup> The optical model potentials needed to generate the distorted waves in the entrance channel were determined by fitting tabulated  $\alpha$ -particle elastic scattering data on  ${}^{12}\text{C}$ ,  ${}^{13}\text{C}$ ,  ${}^{14}\text{N}$ , and  ${}^{15}\text{N}$  at 40.5 MeV (Ref. 40) and on  ${}^{16}\text{O}$  at 65 MeV (Ref. 41) with the search code GENOA.<sup>42</sup> The scattering data for each target were fitted individually with Woods-Saxon potentials having both real and imaginary volume terms. For each of the targets  ${}^{13}\text{C}$ ,  ${}^{14}\text{N}$ , and  ${}^{15}\text{N}$  there was a potential, given in Table IV, which gave the lowest  $\chi^2$  fit to the scattering data on that target. For  ${}^{12}\text{C}$  and  ${}^{16}\text{O}$ , two or more potentials fit the elastic data equally well and thus the one which best reproduced the shape of the  $(\alpha, {}^8\text{Be})$  angular distributions was selected (see Table IV). The sensitivity of the shape of the calculated cross sections to the entrance channel potential made this choice straightforward. For the  ${}^9\text{Be}$ ,  ${}^{10}\text{B}$ , and  ${}^{11}\text{B}$  targets no tabulated scattering data were available in the appropriate energy region. Thus a potential from the literature<sup>43</sup> (similar to the above  ${}^{13}\text{C}$  one, see Table IV) which reproduced 46 MeV  $\alpha$  scattering on  ${}^{11}\text{B}$  was used.

In order to approximate a potential for the par-

ticle-unstable  ${}^8\text{Be}$ , GENOA was used to determine an optical potential which reproduced 50 MeV  ${}^9\text{Be}$  elastic scattering data<sup>44</sup> on  ${}^{12}\text{C}$  (potential AA in Table IV). A second potential with a larger real well depth was also tried. This latter potential caused a small change in the magnitude of the fits and virtually no change in the shape. Since the  ${}^{16}\text{O}(\alpha, {}^8\text{Be}){}^{12}\text{C}$  reaction calculations were found to be relatively insensitive to the exit channel potential and no  ${}^9\text{Be}$  elastic scattering data existed for the other exit channels, potential AA was used to generate the distorted waves in the  ${}^8\text{Be}$  channel for all of the  $1p$  shell targets.

The bound state wave functions which describe the motion of an  $\alpha$  cluster in the target nucleus  $B$  and in  ${}^8\text{Be}$  were calculated in the usual way using a real Woods-Saxon potential whose well-depth was adjusted to give the observed  $\alpha$  binding energy. The radius of the Woods-Saxon well describing the target nuclei was chosen to be  $R = r_0 A^{1/3}$ . An  $r_0$  of 2.0 was used for all targets; this gave a radius which was larger than the physical size of the core  $A$ . This larger radius could correspond to the transferred  $\alpha$  particle existing at the surface of the core. Decreasing  $r_0$  from 2.0 to 1.2 had only a small effect on the shape of the fits but caused a strong decrease in the magnitude of the cross section.

Although  ${}^8\text{Be}$  is unbound by 92 keV, it is effectively bound by its Coulomb barrier during the reaction time. To generate a bound state wave function for the calculations, it was assumed that the  ${}^8\text{Be}$  internal wave function varied smoothly and slowly when its binding energy was changed from  $-92$  to  $+10$  keV. The  ${}^8\text{Be}$  internal wave function was then calculated for an  $\alpha$  particle bound to a second one by 10 keV in a Woods-Saxon well with a radius of 3.2 fm. (Changing the binding energy from 100 to 10 keV produced no change in the shape of the calculated cross sections and only a 7% de-

TABLE IV. Optical model potentials used in the DWBA calculations.

Target	Projectile	$E_{\text{proj}}$ (MeV)	$V$ (MeV)	$r_R^a$ (fm)	$a_R$ (fm)	$W$ (MeV)	$r_I^a$ (fm)	$a_I$ (fm)	$r_C^a$ (fm)	Potential
${}^{16}\text{O}$	$\alpha$	65.0	89.3	1.56	0.57	27.7	1.39	0.72	1.2	A <sup>b</sup>
${}^{15}\text{N}$	$\alpha$	40.5	279.0	1.22	0.65	17.6	1.55	0.65	1.2	B <sup>c</sup>
${}^{14}\text{N}$	$\alpha$	40.5	279.0	1.22	0.65	17.6	1.55	0.65	1.2	B <sup>c</sup>
${}^{13}\text{C}$	$\alpha$	40.5	170.0	1.47	0.55	20.8	1.56	0.35	1.2	C <sup>c</sup>
${}^{12}\text{C}$	$\alpha$	40.5	36.7	1.80	0.41	7.6	1.96	0.66	1.2	D <sup>c</sup>
${}^{11}\text{B}$ , ${}^{10}\text{B}$ , ${}^9\text{Be}$	$\alpha$	46.0	194.0	1.38	0.60	24.0	1.60	0.60	1.2	E <sup>d</sup>
${}^{12}\text{C}$	${}^8\text{Be}$	50.0	35.2	1.72	0.92	12.0	2.65	0.50	1.2	AA <sup>e</sup>

<sup>a</sup>  $R = r_0 A_{\text{tgt}}^{1/3}$ .

<sup>b</sup> Derived from tabulated data in Ref. 41.

<sup>c</sup> Derived from tabulated data in Ref. 40.

<sup>d</sup> Potential for  ${}^{11}\text{B}$  taken from Ref. 43.

<sup>e</sup> Reference 44.

TABLE V. Comparison of experimental and theoretical  $\alpha$ -particle spectroscopic factors.

Target	Level (MeV)	Theory <sup>a</sup>			Experiment	
		$S^0$	$S^2$	$S^4$	$S_{th}$	$S_{exp}$
<sup>16</sup> O	<sup>12</sup> C(g.s.)	0.23			0.23	0.25
	4.44		1.30		1.30	1.07
	7.65	0.06			0.06	0.05
	14.08			2.38	2.38	1.40
<sup>15</sup> N	<sup>11</sup> B(g.s.)		0.41		0.41	0.23
	2.12	0.20			0.20	0.12
	4.44		0.29		0.29	0.29
	6.74			1.09	1.09	0.45
<sup>14</sup> N	<sup>10</sup> B(g.s.)		0.012	0.69	0.70	0.41
	2.15	0.08	0.10		0.18	0.10
	3.59		0.35		0.35	0.14
	4.77		0.044	0.004	0.05	0.04
	6.02			0.40	0.40	0.52
<sup>13</sup> C	<sup>9</sup> Be(g.s.)		0.41		0.41	0.37
	2.43		0.22		0.22	0.18
<sup>12</sup> C	<sup>8</sup> Be(g.s.)	0.56			0.56	0.55
	2.94		0.71		0.71	0.75
<sup>11</sup> B	<sup>7</sup> Li(g.s.)	0.26	0.39		0.65	0.19
	4.63		0.06	0.43	0.49	0.34
<sup>10</sup> B	<sup>6</sup> Li(g.s.)		0.000	0.003	0.003	0.16
	2.18	0.22	0.60	0.24	1.06	0.42
<sup>9</sup> Be	<sup>5</sup> He(g.s.)	0.56	0.56		1.12	0.53

<sup>a</sup> Theoretical  $S_\alpha$  from Kurath (Ref. 9). See Table III for Rotter's  $S_\alpha$  (Ref. 8).

crease in their magnitudes.)

In deriving experimental spectroscopic factors, we have tried to maintain consistent criteria for choosing the center of mass angle at which to relate experiment and theory, since the shapes of the calculated and experimental cross sections are not identical. If an experimental maximum existed in the angular distribution, the theoretical and experimental yields were compared at this angle. For the flatter angular distributions, the spectroscopic factor was calculated at a data point between  $\theta_{c.m.} = 25$  and  $35^\circ$ . A comparison of the experimental  $S_\alpha$  with Kurath's theoretical ones<sup>9</sup> is presented in Table V.

The values of the theoretical  $\alpha$ -particle spectroscopic factors  $S^L(B \rightarrow A + \alpha)$  in Eq. (3) were taken from Kurath<sup>9</sup> and from Rotter.<sup>8</sup> For  $S(^8\text{Be} \rightarrow \alpha + \alpha)$  the theoretical value of 1.5 was taken from Kurath.<sup>9</sup> The calculated cross sections and the experimental data are shown in Figs. 12 to 17 and are discussed in the following section.

#### B. Comparison of theoretical and experimental cross sections

For most nuclei, Kurath's<sup>9</sup> and Rotter's<sup>8</sup> spectroscopic factors are in good agreement. Since

Kurath gives spectroscopic factors for all the  $1p$  shell targets, the theoretical cross sections shown were calculated using his values unless otherwise noted. For Figs. 12–17 the width of each data point corresponds to the angular acceptance of the <sup>8</sup>Be identifier used in the measurement. Furthermore, if the statistical error exceeded the height of the data point, it is given in the figure.

#### 1. <sup>16</sup>O( $\alpha$ ,<sup>8</sup>Be)<sup>12</sup>C

A comparison of the ( $\alpha$ ,<sup>8</sup>Be) experimental (symbols) and absolute calculated (solid curves) cross sections for transitions populating the <sup>12</sup>C ground state and several excited states is shown in Fig. 12. The similar magnitudes of the experimental and calculated cross sections demonstrate good agreement between the theoretical  $\alpha$ -particle spectroscopic factors and experiment (see Table

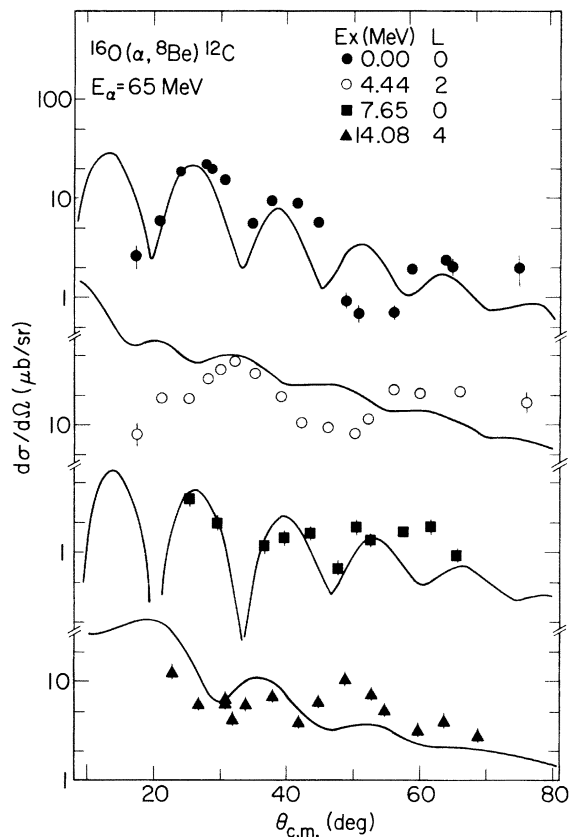


FIG. 12. Absolute experimental (symbols) and calculated (solid curves) ( $\alpha$ ,<sup>8</sup>Be) cross sections at  $E_\alpha = 65$  MeV for transitions populating the <sup>12</sup>C(g.s.) and several excited states. In this figure and the following ones containing experimental angular distributions, a statistical error is given if it exceeds the height of the data point. In addition, the width of each data point corresponds to the angular acceptance of the <sup>8</sup>Be identifier used in measuring that point.

V). The shapes of the theoretical cross sections reproduce some of the features of the experimental data—most notably the relative spacing and magnitude of the two forward maxima in the ground state angular distribution. Furthermore, the damping of the oscillatory character observed experimentally in the  $L=2$  and  $L=4$  angular distributions, compared with that of the  $L=0$  ground state, is also reproduced by the calculations.

## 2. ${}^{15}\text{N}(\alpha, {}^8\text{Be}){}^{11}\text{B}$

For the  ${}^{15}\text{N}$  target the magnitudes of the experimental and theoretical cross sections are generally in fair agreement (see Fig. 13). The structureless shapes of the experimental  $L=2$  and  $L=4$  angular distributions are qualitatively reproduced by the calculations, but the theoretical  $L=0$  angular distribution shows more pronounced oscillations than does experiment.

Over the very limited angular range studied on the  ${}^{14}\text{N}$  target the experimental cross sections are structureless and relatively constant (see Fig. 14). The theoretical calculations generally reproduce this feature as well as the cross section magnitudes. It should be noted that all of these transi-

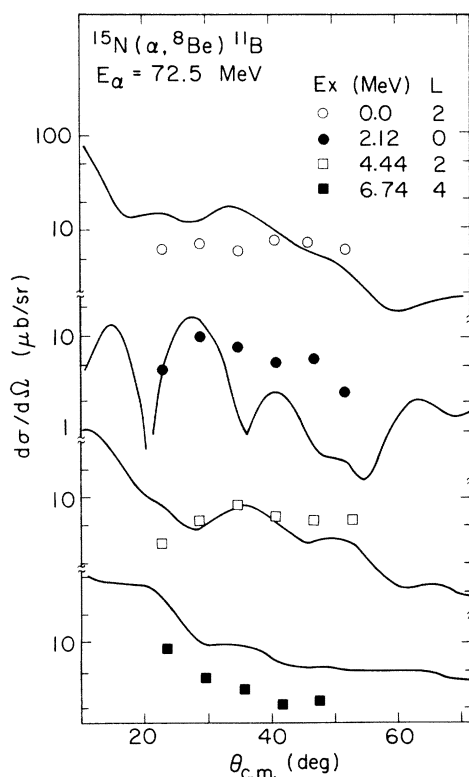


FIG. 13. Absolute experimental (symbols) and theoretical (solid curves)  $(\alpha, {}^8\text{Be})$  cross sections at  $E_\alpha = 72.5$  MeV for transitions populating the  ${}^{11}\text{B}(\text{g.s.})$  and three excited states.

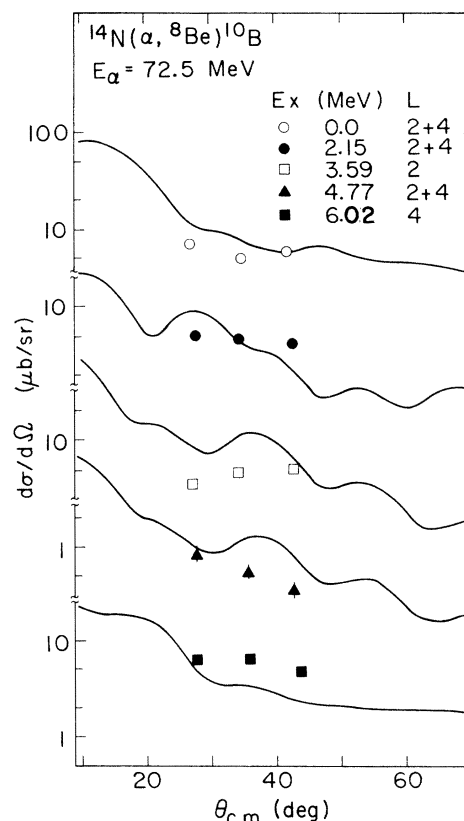


FIG. 14. Absolute experimental (symbols) and theoretical (solid curves)  $(\alpha, {}^8\text{Be})$  cross sections at  $E_\alpha = 72.5$  MeV for transitions populating the  ${}^{10}\text{B}(\text{g.s.})$  and four excited states.

tions to  ${}^{10}\text{B}$  have an angular momentum transfer of 2 or greater. For transitions involving two  $L$  values, the incoherent sum of the contributions to the cross section from both values is shown in Fig. 14.

## 3. ${}^{13}\text{C}(\alpha, {}^8\text{Be}){}^9\text{Be}$

The structureless shapes of the  ${}^{13}\text{C}$  data (see Fig. 15) are reproduced by the calculated cross sections although the yields are overestimated at forward angles and underestimated at backward ones. The shapes of the angular distributions observed from the  ${}^{12}\text{C}$  target (see Fig. 15) are poorly reproduced by the fits which severely overestimate the magnitude of the cross section at forward angles. However, the magnitudes do agree in the region of the experimentally observed maxima near  $40^\circ$ .

## 4. ${}^{11}\text{B}(\alpha, {}^8\text{Be}){}^7\text{Li}$ and ${}^9\text{Be}(\alpha, {}^8\text{Be}){}^5\text{He}$

For the  ${}^{11}\text{B}$ ,  ${}^{10}\text{B}$ , and  ${}^9\text{Be}$  targets, two or more values of  $L$  are allowed. Figure 16 shows two examples which illustrate the relative contributions

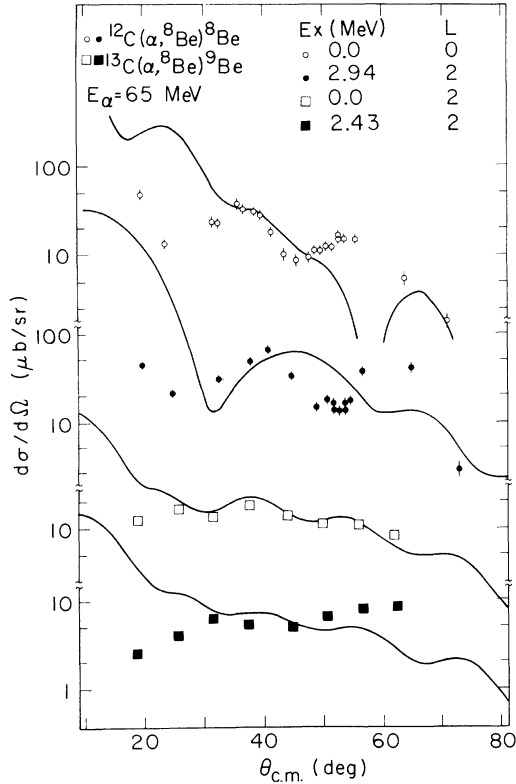


FIG. 15. Absolute experimental (symbols) and theoretical (solid curves)  $(\alpha, {}^8\text{Be})$  cross sections at  $E_\alpha = 65$  MeV for transitions populating the  ${}^9\text{Be}(\text{g.s.})$  and first excited state plus the  ${}^9\text{Be}(\text{g.s.})$  and an excited state.

from each  $L$  value to the shape and magnitude of the theoretical cross section (Rotter's<sup>8</sup> values of  $S^L$  were used). The transition to the  ${}^6\text{Li}$  ground state can proceed by the pickup of an  $\alpha$  particle with an angular momentum of 2 or 4 with the  $L = 4$  component making the dominant contribution; for the  ${}^7\text{Li}(\text{g.s.})$ ,  $L = 0$  or 2, with the  $L = 2$  component dominant. Since the kinematic factors for  $L = 0$ , 2, or 4 transfer are comparable, the magnitude of the cross section for a particular  $L$  value in these two cases directly reflects the magnitude of the theoretical  $S_\alpha$ .

For reactions on  ${}^{10}\text{B}$  the theoretical  $S_\alpha$  of Kurath and of Rotter differ somewhat, though for reactions on  ${}^9\text{Be}$  and  ${}^{11}\text{B}$  they are very similar (see Table III). In Fig. 17, calculated curves using both Kurath's<sup>9</sup> (solid) and Rotter's<sup>8</sup> (dashed)  $S_\alpha$  are presented. Disagreement with experiment is greatest for the transition to the  ${}^6\text{Li}(\text{g.s.})$ ; however, the difference is small in absolute magnitude since the transition is predicted to be very weak. The magnitudes of the calculated cross sections are roughly comparable to the experimental ones for the transitions to the  ${}^6\text{Li}(2.18 \text{ MeV})$ ,  ${}^7\text{Li}(\text{g.s.})$ , and  ${}^7\text{Li}(4.63 \text{ MeV})$  states; however, the flatness

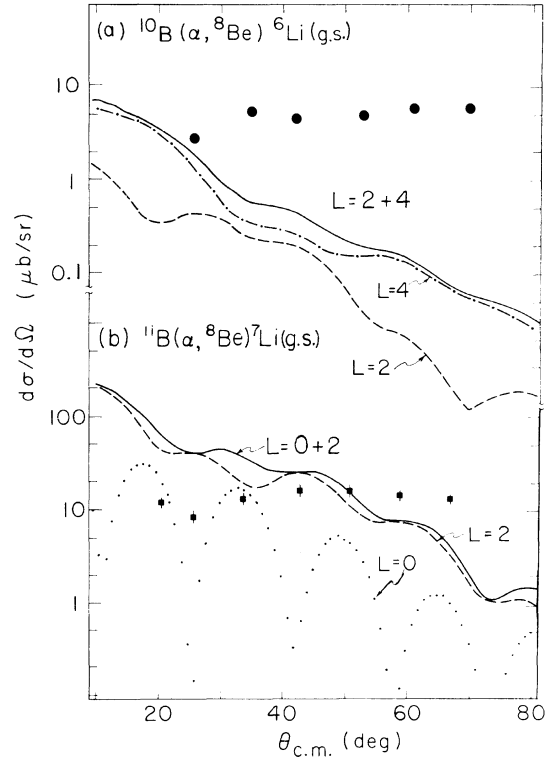


FIG. 16. An illustration for the  ${}^{10}\text{B}(\alpha, {}^8\text{Be}){}^6\text{Li}(\text{g.s.})$  and  ${}^{11}\text{B}(\alpha, {}^8\text{Be}){}^7\text{Li}(\text{g.s.})$  reactions at 72.5 MeV of the relative contributions of different  $L$  values to the theoretical cross sections [Rotter's (Ref. 8) values of  $S^L$  were used]. The theoretical curves for each  $L$  value are labeled and the sum of the contributions of both possible  $L$  values is given by the solid lines (see text).

of the experimental data is not reproduced. For the very limited  ${}^9\text{Be}$  target data the theoretical curve follows the slope but overestimates the magnitude of the differential cross sections. The poorer quality<sup>45</sup> fits for the reactions on the  ${}^9\text{Be}$ ,  ${}^{10}\text{B}$ , and  ${}^{11}\text{B}$  targets could be due in part to the fact that the exit channel elastic scattering may not be well described by potential AA (see Table IV), which was obtained from  ${}^9\text{Be}$  scattering on  ${}^{12}\text{C}$ . In addition the reaction calculations are sensitive to the entrance channel optical parameters, but  $\alpha$ -particle scattering data on  ${}^9\text{Be}$  and  ${}^{10}\text{B}$  were not available and thus potential E (derived from  $\alpha$  scattering on  ${}^{11}\text{B}$ ) was used of necessity.

### C. General comparison of theoretical and experimental $\alpha$ -particle spectroscopic factors

In Fig. 18(a) are shown ratios  $R^{\text{abs}}$  of experimental to theoretical  $S_\alpha$  (see also Table V) where  $R^{\text{abs}}$  is defined by

$$R^{\text{abs}} = \frac{S(\text{exp})}{S(\text{theory})} = \frac{d\sigma/d\Omega(\theta)_{\text{exp}}}{d\sigma/d\Omega(\theta)_{\text{th}}} \quad (4)$$



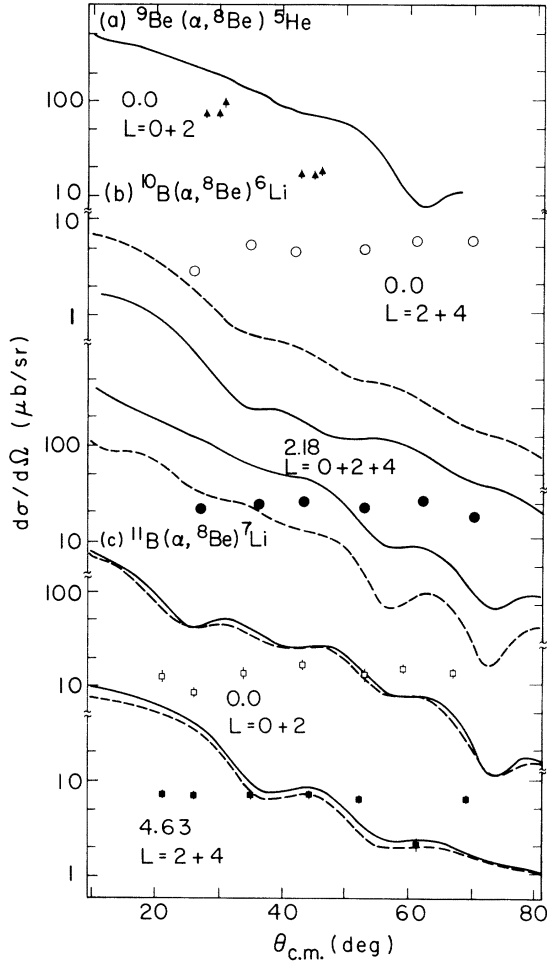


FIG. 17. Experimental (symbols) and theoretical (curves)  $(\alpha, {}^8\text{Be})$  cross sections at  $E_\alpha = 65$  MeV ( ${}^9\text{Be}$  and  ${}^{11}\text{B}$ ) and at  $E_\alpha = 72.5$  MeV ( ${}^{10}\text{B}$ ) for transitions populating (a) the  ${}^5\text{He}(\text{g.s.})$ , (b) the  ${}^6\text{Li}(\text{g.s.})$  and 2.18 MeV state, and (c) the  ${}^7\text{Li}(\text{g.s.})$  and 4.63 MeV state (see text). These theoretical cross sections were calculated with  $S_\alpha$  from both Kurath (Ref. 9) (solid lines) and Rotter (Ref. 8) (dashed lines).

For consistency, Kurath's theoretical  $\alpha$ -particle spectroscopic factors<sup>9</sup> are used for all targets. In general these ratios lie below the dashed line at  $R^{\text{abs}} = 1.0$ , but deviate from it by less than 50%. (Of course, this comparison is very sensitive to systematic errors either in the experimental data or in the reaction calculations; an example of the latter is that the magnitude of the calculated cross section is affected by the value of  $r_0$  used in calculating the bound state wave functions). The  ${}^6\text{Li}(\text{g.s.})$  point is off scale because of its very small theoretical  $S_\alpha$ .

In order to minimize systematic errors, the above ratio of spectroscopic factors,  $R^{\text{abs}}$ , was divided by the ratio for the ground state transition.

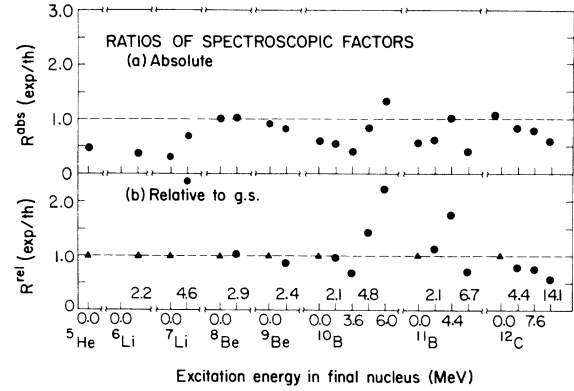


FIG. 18. (a) A comparison of the ratios of experimental to Kurath's (Ref. 9) theoretical spectroscopic factors [ $R^{\text{abs}} = S(\text{exp})/S(\text{theory})$ ]. (b) A comparison of these ratios relative to the ground state ratio for each target (see discussion in text). Note that the ratio ( $R^{\text{rel}}$ ) of  $S_\alpha$  relative to the 2.2 MeV state in  ${}^6\text{Li}$  is given for  ${}^{10}\text{B} \rightarrow {}^6\text{Li} + \alpha$ . In both parts (a) and (b), the  ${}^6\text{Li}(\text{g.s.})$  point is off scale because of its very small theoretical  $S_\alpha$  (see Tables V and VI).

TABLE VI. Comparison of experimental and theoretical relative  $\alpha$ -particle spectroscopic factors.

Target	Level	Theory <sup>a</sup>	$S_\alpha^{\text{rel}}$ Experiment
${}^{16}\text{O}$	${}^{12}\text{C}(\text{g.s.})$	1.00	1.00
	4.44	5.54	4.28
	7.65	0.26	0.20
	14.08	10.15	5.60
${}^{15}\text{N}$	${}^{11}\text{B}(\text{g.s.})$	1.00	1.00
	2.12	0.50	0.52
	4.44	0.72	1.26
	6.74	2.68	1.96
${}^{14}\text{N}$	${}^{10}\text{B}(\text{g.s.})$	1.00	1.00
	2.14	0.25	0.24
	3.59	0.50	0.34
	4.77	0.07	0.10
	6.02	0.58	1.27
${}^{13}\text{C}$	${}^9\text{Be}(\text{g.s.})$	1.00	1.00
	2.43	0.53	0.49
${}^{12}\text{C}$	${}^8\text{Be}(\text{g.s.})$	1.00	1.00
	2.94	1.28	1.36
${}^{11}\text{B}$	${}^7\text{Li}(\text{g.s.})$	1.00	1.00
	4.63	0.75	1.79
${}^{10}\text{B}$	${}^6\text{Li}(\text{g.s.})$	0.003 <sup>b</sup>	0.38 <sup>b</sup>
	2.18	1.00	1.00
${}^9\text{Be}$	${}^5\text{He}(\text{g.s.})$	1.00	1.00

<sup>a</sup> Theoretical  $S_\alpha$  from Ref. 9.

<sup>b</sup> The ratio of  $S_\alpha$  relative to the 2.18 MeV state is given for  ${}^{10}\text{B} \rightarrow {}^6\text{Li} + \alpha$ .

TABLE VII. Comparison of theoretical and experimental ground state  $\alpha$ -particle spectroscopic factors normalized to unity for  $S_\alpha[{}^{12}\text{C} \rightarrow {}^8\text{Be}(\text{g.s.}) + \alpha]$ .

Target	Theoretical			$S_\alpha^{\text{rel}}$ Experimental						
	Kurath <sup>a</sup>	Rotter <sup>b</sup>	This <sup>c</sup> work ( $\alpha, {}^8\text{Be}$ )	Gutbrod <sup>d</sup>	Bedjidian <sup>e</sup> ( $d, {}^6\text{Li}$ )	Denes <sup>f</sup>	Detraz <sup>g</sup>	Audi <sup>h</sup> ( ${}^3\text{He}, {}^7\text{Be}$ )	Steele <sup>i</sup>	Sherman ( $\alpha, 2\alpha$ )
${}^9\text{Be}$	2.00	2.12	0.96							
${}^{10}\text{B}$	0.005	0.024	0.29	0.33						
${}^{11}\text{B}$	1.17	1.02	0.35	1.62						
${}^{12}\text{C}$	1.00	1.00	1.00	1.00	1.00	1.00	1.00	1.00	1.00	1.00
${}^{13}\text{C}$	0.73		0.67			2.0			0.44	
${}^{14}\text{N}$	1.25		0.75							
${}^{15}\text{N}$	0.73		0.42							
${}^{16}\text{O}$	0.41	0.42	0.44	0.44	0.32	5.0	3.3	0.64 <sup>k</sup>	0.97	1.21

<sup>a</sup> Theoretical  $S_\alpha$  from Ref. 9.

<sup>b</sup> Theoretical  $S_\alpha$  from Ref. 8.

<sup>c</sup> This work ( $\alpha, {}^8\text{Be}$ ) at 65–72.5 MeV.

<sup>d</sup> See Ref. 13, ( $d, {}^6\text{Li}$ ) at 19.5 MeV.

<sup>e</sup> See Ref. 46, ( $d, {}^6\text{Li}$ ) at 28 MeV.

<sup>f</sup> See Ref. 47, ( $d, {}^6\text{Li}$ ) at 15 MeV.

<sup>g</sup> See Ref. 48, ( ${}^3\text{He}, {}^7\text{Be}$ ) at 30 MeV.

<sup>h</sup> See Ref. 14, ( ${}^3\text{He}, {}^7\text{Be}$ ) at 26 MeV.

<sup>i</sup> See Ref. 15, ( ${}^3\text{He}, {}^7\text{Be}$ ) at 70 MeV.

<sup>j</sup> See Ref. 16, ( $\alpha, 2\alpha$ ) at 90 MeV.

<sup>k</sup> Average of numbers given in Ref. 14.

The ratio  $R^{\text{rel}}$  is defined by:

$$R^{\text{rel}} = \frac{R^{\text{abs}}(B \rightarrow A + \alpha)}{R^{\text{abs}}[B \rightarrow A(\text{g.s.}) + \alpha]}. \quad (5)$$

Part (b) of Fig. 18 presents this relative ratio of  $S_\alpha$ ;  $R^{\text{rel}}$  is again plotted against the final state populated. Only four values of  $R^{\text{rel}}$  are farther than  $\pm 50\%$  from unity; the  ${}^6\text{Li}(\text{g.s.})$  point is again off scale. Relative spectroscopic factors for the individual transitions are also presented in Table VI.

Several previous investigators have measured  $\alpha$ -particle spectroscopic factors for the ground state to ground state transitions utilizing the ( $d, {}^6\text{Li}$ ), ( ${}^3\text{He}, {}^7\text{Be}$ ), and ( $\alpha, 2\alpha$ ) reactions on  $1p$  shell targets. These results were typically reported as relative spectroscopic factors normalized to 1 for the  ${}^{12}\text{C} \rightarrow {}^8\text{Be}(\text{g.s.})$  transition. In Table VII<sup>46–48</sup> two theoretical and several experimental  $S_\alpha$  are compared [with  $S({}^{12}\text{C} \rightarrow {}^8\text{Be}(\text{g.s.}) + \alpha) = 1$ ]; it can be seen that the two theoretical predictions are very similar.

Comparing the experimental spectroscopic factors with the theoretical ones, it is clear that the ( $\alpha, {}^8\text{Be}$ ) results are in moderate agreement with theory, particularly on the heavier targets. Some scatter is observable in the various ( $d, {}^6\text{Li}$ ), ( ${}^3\text{He}, {}^7\text{Be}$ ), and ( $\alpha, 2\alpha$ ) data in the table. However, the agreement among some of the experimental measurements is encouraging considering the dif-

ferent reactions and the wide range of bombarding energies employed. The experimentally observed strength to the  ${}^6\text{Li}(\text{g.s.})$  may indicate that  ${}^{10}\text{B}$  has a larger amount of this parentage than is theoretically predicted; however, since this transition is predicted to be very weak, other reaction mechanisms which are normally negligible could account for some of the observed strength.

## V. SUMMARY AND CONCLUSIONS

An investigation of the ( $\alpha, {}^8\text{Be}$ ) reaction at high bombarding energies on all stable  $1p$  shell target nuclei has been presented. This study has shown that the ( $\alpha, {}^8\text{Be}$ ) reaction can be understood in terms of a simple  $\alpha$ -cluster pickup process which has been previously used to describe successfully the major features of the ( $d, {}^6\text{Li}$ ) and ( ${}^3\text{He}, {}^7\text{Be}$ ) reactions. A systematic feature which emerged from this investigation was the strong population of only those states which are predicted to have significant  $\alpha$ -particle spectroscopic factors. This selectivity is evidence that the ( $\alpha, {}^8\text{Be}$ ) reaction proceeds via a simple  $\alpha$ -cluster pickup process. The relative population of final states via the ( $\alpha, {}^8\text{Be}$ ) reaction on  $1p$  shell nuclei was generally in good agreement with the previously reported ( $d, {}^6\text{Li}$ ) and ( ${}^3\text{He}, {}^7\text{Be}$ ) results. However, a notable exception to this arose in that, while no population of the mixed isospin states at  $\sim 16$  MeV in  ${}^8\text{Be}$  by

the  ${}^{12}\text{C}(\alpha, {}^8\text{Be})$  reaction was expected or observed, both the  $(d, {}^6\text{Li})$  and  $({}^3\text{He}, {}^7\text{Be})$  reactions moderately populate these levels of dominant single-particle character.

The probable occurrence of a cluster pickup mechanism for the  $(\alpha, {}^8\text{Be})$  reaction greatly simplifies the theoretical description. In order to extract  $\alpha$ -particle spectroscopic factors for comparison with theory, the data were analyzed with exact-finite-range DWBA. These reaction calculations were found to be sensitive to the optical potential describing the entrance channel elastic scattering, but rather insensitive to the exit channel potential. Both absolute and relative spectroscopic factors were extracted for 22 states which are generally in good agreement with the theoretical predictions of both Kurath<sup>9</sup> and Rotter<sup>8</sup> as to the extent of  $\alpha$  clustering in these light nuclei.

The selectivity and good quantitative agreement with theoretical predictions illustrate that the  $(\alpha, {}^8\text{Be})$  reaction is a useful spectroscopic probe with which to measure the extent of  $\alpha$  clustering in nuclei. Furthermore, the large solid angle  ${}^8\text{Be}$  identifier described within will facilitate similar studies on heavier nuclei.

#### ACKNOWLEDGMENTS

We wish to thank D. Landis for designing the fast/slow preamplifiers, J. Walton for fabricating the transmission detectors, Dr. M. Nagarajan for many informative discussions on direct reaction theory and for his keen interest throughout the duration of this work, and Dr. George Delic for checking some of our EFR-DWBA calculations with his reaction code KUNDRY and for several helpful discussions on optical model potentials.

\*Work performed under the auspices of the U. S. Energy Research and Development Administration.

<sup>1</sup>E. P. Wigner, Phys. Rev. **51**, 106 (1937).

<sup>2</sup>D. H. Wilkinson, in *Proceedings of the Rutherford Jubilee International Conference, Manchester*, 1961, edited by J. Birks (Heywood and Company, Ltd., London 1961), p. 339.

<sup>3</sup>G. A. Wheeler, Phys. Rev. **52**, 1083 (1937).

<sup>4</sup>K. Wildermuth and W. McClure, in *Springer Tracts in Modern Physics* (Springer-Verlag, Berlin, Heidelberg, New York, 1966), Vol. 41.

<sup>5</sup>D. M. Brink, in *Proceedings of the International School of Physics, "Enrico Fermi," 1965, Course 36*, edited by C. Bloch (Academic, New York, 1966), p. 247.

<sup>6</sup>A. Arima, H. Horiuchi, K. Kubodera, and N. Takigawa, in *Advances in Nuclear Physics*, edited by M. Baranger and E. Vogt (Plenum, New York, 1973), Vol. 5, p. 345.

<sup>7</sup>D. M. Brink, in *Proceedings of the Second International Conference on Clustering Phenomena in Nuclei*, College Park, Maryland, 1975 [U. S. ERDA Report No. ORO-4856-26 (unpublished)], p. 3. Also, see other references in these proceedings.

<sup>8</sup>I. Rotter, Fortschr. Phys. **16**, 195 (1968).

<sup>9</sup>D. Kurath, Phys. Rev. C **7**, 1390 (1973).

<sup>10</sup>K. Bethge, Annu. Rev. Nucl. Sci. **20**, 255 (1970).

<sup>11</sup>J. D. Garrett, in the *Proceedings of the Symposium on Two-Nucleon Transfer and Pairing Excitations* [Argonne Physics Division Informal Report No. PHY-1972H, 1972 (unpublished)], p. 232].

<sup>12</sup>F. D. Becchetti, L. T. Chua, J. Jänecke, and A. M. Vandermolen, Phys. Rev. Lett. **34**, 225 (1975).

<sup>13</sup>H. H. Guthbrod, H. Yoshida, and R. Bock, Nucl. Phys. **A165**, 240 (1971).

<sup>14</sup>G. Audi, C. Détraz, M. Langevin, and F. Pougheon, Nucl. Phys. **A237**, 300 (1975).

<sup>15</sup>W. F. Steele, P. A. Smith, J. E. Finck, and G. M. Crawley, Michigan State University Report No. MSUCL-186, 1975 (unpublished).

<sup>16</sup>J. D. Sherman, D. L. Hendrie, and M. S. Zisman, Phys.

Rev. C **13**, 20 (1976).

<sup>17</sup>R. E. Brown, J. S. Blair, D. Bodansky, N. Cue, and C. D. Kavaloski, Phys. Rev. **138**, B1394 (1965).

<sup>18</sup>G. J. Wozniak, N. A. Jelley, and J. Cerny, Phys. Rev. Lett. **31**, 607 (1973).

<sup>19</sup>G. J. Wozniak, N. A. Jelley, and J. Cerny, Nucl. Instrum. Methods **120**, 29 (1974).

<sup>20</sup>F. Brochard, P. Chevallier, D. Disdier, V. Rauch, G. Rudolf, and F. Scheibling, Phys. Rev. C **13**, 967 (1976).

<sup>21</sup>K. S. Jayaraman and H. D. Holmgren, Phys. Rev. **172**, 1015 (1968).

<sup>22</sup>G. J. Wozniak, H. L. Harney, K. H. Wilcox, and J. Cerny, Phys. Rev. Lett. **28**, 1278 (1972).

<sup>23</sup>J. G. Cramer, K. A. Eberhard, N. R. Fletcher, E. Mathiak, H. H. Rossner, and A. Weidinger, Nucl. Instrum. Methods **111**, 425 (1973).

<sup>24</sup>J. L. Artz, M. B. Greenfield, and N. R. Fletcher, Phys. Rev. C **13**, 156 (1976).

<sup>25</sup>H. Ho, W. Dunnweber, D. Dehnhard, K. Mudersbach, and J. P. Wurm, Nucl. Phys. **A233**, 361 (1974).

<sup>26</sup>A. Menchaca-Rocha, Nucl. Instrum. Methods **114**, 425 (1974).

<sup>27</sup>Tests with an  $\alpha$ -particle source demonstrated that no false coincidences were generated by particles passing through the 1 mm dead region between the twin  $\Delta E$  detectors and thus collimation of this region was unnecessary.

<sup>28</sup>Due to the very low background attainable with the  $\Delta TOF$  and  $PI$  requirements, a comparison of the energy losses in the twin  $\Delta E$  detectors was not used; this approach is discussed in Ref. 19.

<sup>29</sup>Our PSD's were obtained from Edax International, Inc. <sup>30</sup>Copies of this program are available from the authors upon request.

<sup>31</sup>Quoted excitation energies, spin and parity assignments for states in  ${}^{12}\text{C}$  and  ${}^{11}\text{B}$  are taken from F. Ajzenberg-Selove, Nucl. Phys. **A248**, 1 (1975).

<sup>32</sup>Quoted excitation energies, spin and parity assign-

- ments for states in  $^{10}\text{B}$ ,  $^9\text{Be}$ ,  $^8\text{Be}$ ,  $^7\text{Li}$ ,  $^6\text{Li}$ , and  $^5\text{He}$  are taken from F. Ajzenberg-Selove and T. Lauritsen, Nucl. Phys. A227, 1 (1974).
- <sup>33</sup>J. Lowe, A. R. Polletti, and D. H. Wilkinson, Phys. Rev. 148, 1045 (1966).
- <sup>34</sup>A. A. Pilt (private communication).
- <sup>35</sup>J. B. Marion and M. Wilson, Nucl. Phys. 77, 129 (1966).
- <sup>36</sup>M. A. Nagarajan, Phys. Lett. 52B, 395 (1974).
- <sup>37</sup>R. L. McGrath, D. L. Hendrie, E. A. McClatchie, B. G. Harvey, and J. Cerny, Phys. Lett. 34B, 289 (1971).
- <sup>38</sup>N. S. Chant and P. G. Roos, in Proceedings of the Second International Conference on Clustering Phenomena in Nuclei, College Park, Maryland, 1975 (see Ref. 7), p. 265.
- <sup>39</sup>R. M. DeVries, Phys. Rev. C 8, 951 (1973).
- <sup>40</sup>B. G. Harvey, J. R. Meriwether, J. Mahoney, A. Busiere de Nercy, and D. J. Horen, Phys. Rev. 146, 712 (1966). See University of California Radiation Laboratory Report No. UCRL-16573 (unpublished) for tabulated data.
- <sup>41</sup>B. G. Harvey, E. J.-M. Rivet, A. Springer, J. R. Meriwether, W. B. Jones, J. H. Elliott, and P. Darriulat, Nucl. Phys. A52, 465 (1964); D. L. Hendrie (private communication).
- <sup>42</sup>F. G. Perey, optical-model search code (unpublished).
- <sup>43</sup>B. Zeidman, H. T. Fortune, and A. Richter, Phys. Rev. C 2, 1612 (1970).
- <sup>44</sup>D. P. Stahel, G. J. Wozniak, B. D. Jeltema, M. S. Zisman, R. Jahn, and J. Cerny, Lawrence Berkeley Laboratory Report No. LBL-5075, 1976 (unpublished).
- <sup>45</sup>A further complication arises in the ( $\alpha$ ,  $^8\text{Be}$ ) reaction on  $^9\text{Be}$ ,  $^{10}\text{B}$ , and  $^{11}\text{B}$  targets in that contributions are possible from simple pickup reactions—i.e.,  $^{10}\text{B}(\alpha, ^6\text{Li})^8\text{Be}$ —in the backward hemisphere. Unfortunately, no data are available for this bombarding energy and angular region from which to estimate their contribution.
- <sup>46</sup>M. Bedjidian, M. Chevallier, J. Y. Grossiord, A. Guichard, M. Gusakov, J. R. Pizzi, and C. Ruhla, Nucl. Phys. A189, 403 (1972).
- <sup>47</sup>L. J. Denes, W. W. Daehnick, and R. M. Drisko, Phys. Rev. 148, 1097 (1966).
- <sup>48</sup>C. Détraz, H. H. Duhm, and H. Hafner, Nucl. Phys. A147, 488 (1970).